energies

MDPI

Article

Pinch-Point Targeting of Organic Rankine Cycle Waste-Heat Recovery from the Exhaust Streams of a Cement Plant: A Numerical Study on Measured Plant Data and the Effect of False Air

Faisal Albatati

Mechanical Engineering Department, Faculty of Engineering, King Abdulaziz University, Rabigh 25732, Saudi Arabia; alalbatati@kau.edu.sa

Abstract

Pinch analysis and cycle modeling assess heat recovery from the measured preheater, bypass and cooler exhaust streams of a dry-process cement line, which release 39.85 MW above 150 °C with the raw mill stopped. At a 5 K minimum approach in the source exchangers, the evaluated cycles have nominal net power targets of 10.49 MW for supercritical cyclopentane, 10.43 MW for cyclohexane, 10.11 MW for toluene, and 10.00 and 8.28 MW for toluene–cyclohexane 50/50 and n-pentane–toluene 30/70 by mass. The minimum approach lies at the bubble point in the subcritical cycles and at the 227 °C composite breakpoint for cyclopentane. The steam reference gives 9.25 MW at its adopted 120 K superheat bound; the extended search reaches 9.32 MW at 144.6 K. Cyclopentane's 0.063 MW lead over cyclohexane is smaller than twice the paired standard uncertainty, so their ranking remains unresolved. For single-stage turbines, applying a screening threshold of 50 to the volume flow ratio leaves cyclohexane with the highest power target of 9.61 MW; no cyclopentane design meets that threshold within the search domain. In series, three source exchangers transfer 83 to 89% of the heat targets at target mass flows; idealized split flow comes within 0.2% of the power targets. Modeled removal of 5983 Nm^3/h of excess false air from the preheater raises the reoptimized targets nominally by 0.09 to 0.14 MW. At retained cycle states and recalculated mass flows, only the paired gain of steam exceeds twice its standard uncertainty. False air reduction remains primarily a fuel-saving measure.

Keywords: pinch-point analysis; waste-heat recovery; cement plant; organic Rankine cycle; numerical modeling; zeotropic mixture; supercritical cycle; false air; exergy

1. Introduction

Cement manufacture is among the most energy intensive industrial processes. In a dry-process cement line, about 35 to 40% of the process heat is lost with the flue gases and the clinker cooling air [1,2], and these gases are the medium-temperature source that waste-heat power plants use. The thermodynamic cycles applied to cement plants have been reviewed recently [3]. The steam Rankine cycle is a conventional option for cement waste-heat recovery [1,2], whereas organic Rankine cycles (ORCs) and Kalina cycles are applied where the source temperature or the plant scale favors them [1,4]. In a line with a kiln gas bypass, which diverts part of the kiln gas around the preheater, the bypass gas after its quench is a third exhaust stream beside the preheater exit gas and the cooler exhaust air; it carries the bypass residue, which is enriched in chlorides and potassium [5].

In an ORC, the working fluid takes its heat from the heat source in an exchanger, termed here the source exchanger. In the ORC studies reviewed here, the selection of the working

Check for updates

Academic Editor: Silvia Ravelli

Received: 29 September 2026
Revised: 19 October 2026
Accepted: 19 October 2026
Published: 22 October 2026

Copyright: © 2026 by the author. Licensee MDPI, Basel, Switzerland. This article is an open access article distributed under the terms and conditions of the Creative Commons Attribution (CC BY) license.

fluid and its temperature match with the heat source are central design issues [6–8]. At a fixed subcritical pressure, a pure fluid evaporates at a constant temperature. The bubble point marks the start of evaporation, but the location of the minimum temperature difference in the source exchanger, its pinch point, must be identified along the complete heating path. A zeotropic mixture, in contrast, evaporates over a temperature glide, the temperature range between its bubble point and its dew point, where evaporation is complete, so that its evaporation temperature can follow the falling temperature of a cooling gas. Several ORC studies [9–11] have investigated zeotropic mixtures as working fluids because their glide can reduce the exergy destroyed in the source exchanger. A supercritical fluid, heated at a pressure above its critical pressure, has no phase change and no evaporation plateau; its temperature rises along a continuous curve, and the reported advantage of the supercritical cycle over the subcritical cycle is a closer temperature match with the source [6].

Raksa-in et al. [12] compared subcritical, supercritical and zeotropic mixture cycles, together with the trilateral flash and Kalina cycles, under identical heat-source conditions from 100 to 300 °C. In such comparisons, the thermal stability of the organic fluids sets the upper temperature limit: toluene is reported to be stable to about 400 °C, cyclopentane to about 300 °C and n-pentane to about 315 °C [13–15]. For cement exhaust in particular, Fergani et al. [16,17] optimized pure fluids and cyclohexane–toluene and benzene–toluene mixtures on a single exhaust stream at 350 °C, whose heat was supplied to the cycle through an oil loop.

For a heat source made of several streams, pinch analysis provides the targeting framework. The composite curve, which adds the heat released by the streams at each temperature, and the grand composite curve, which shows at each shifted temperature the net heat surplus that the streams pass to lower temperatures (Section 3.4), set the heat recovery targets [18]. Under the appropriate placement principle of Townsend and Linnhoff [19], a heat engine is placed entirely on one side of the process pinch, the temperature that divides the process into a net heat sink above it and a net heat source below it. Pinch-based ORC design methods select the evaporation level against the temperature profile of the source and choose the cycle conditions and the mass flow that keep the prescribed temperature difference from the source; they differ in how they fix the evaporation level and in how they treat the inlet and outlet temperatures of the source. Chen et al. [20] constrained the inlet and outlet temperatures of the heat carrier and coupled them to the source in the design of the cycle. Ryms et al. [21] adapted pinch-point analysis to the ORC design process, and Sarkar [22] built an exergetic optimization of the subcritical ORC based on the pinch-point method. Manalac et al. [23] characterized, by pinch-point analysis, the heat recovery in the evaporator of a partial evaporating cycle with an ejector on cement flue gas. Stijepović et al. [24] used exergy composite curves to design multi-pressure cycles.

With an actual heat exchanger network, approaching heat recovery targets can require changes to the network topology and the arrangement of the exchangers [18,25], and Lee et al. [26] synthesized multi-cycle ORC systems together with a heat exchanger network for low-grade heat. In the cement industry, pinch analysis has been applied by Mian et al. [27] to a process model of cement production; their heat cascade, in which the heat surplus of each temperature interval passes to the next lower interval, was adapted to gas–solid heat exchange, and the heat recovery was formulated as a mixed-integer linear program. Han et al. [28] applied pinch and exergy analysis to the steam waste-heat plant of a 2500 t/d clinker line and obtained a theoretical gain of 7.6% and a measured gain of 5.0% in power generation.

The cement waste-heat recovery studies built on plant data differ in the streams they use, in the origin of their inputs and in the system they place at the source. Khurana et al. [2] drew the energy balance of a 3800 t/d plant from its operating data and estimated that a steam cycle on its waste-heat streams could generate about 4.4 MW, about 30% of

the electricity requirement of the plant. Wang et al. [29] compared single-flash steam, dual-pressure steam, and organic Rankine and Kalina cycles on the preheater and cooler exhausts of a plant by exergy analysis and parametric optimization and found that the Kalina cycle was best under their conditions. Karellas et al. [1] compared a water-steam Rankine cycle with an ORC by energy and exergy analysis and found the steam cycle more efficient for exhaust gases above 310 °C. Kizilkan [30] compared a steam Rankine cycle with a supercritical carbon dioxide Brayton cycle on cement-plant exhaust. Mahmoud et al. [4] obtained a power output of 7.35 MW from the waste heat of the kiln shell, preheater and cooler of a plant in a combined Kalina cycle, against 6.86 MW for separate recovery.

In addition, Sanaye et al. [31] designed and optimized the recovery cycle of a cement plant with its thermoeconomic and environmental assessment, and Amarasinghe et al. [32] measured the heat available in the raw meal department of a plant. More recently, Akroot et al. [33] compared organic Rankine, single-flash steam and dual-pressure steam systems on the preheater and cooler exhausts using the operating data of a plant, and Khafajah et al. [34] matched a cascade ORC to these two exhausts in a trigeneration system for power, cooling and desalination. The plant studies reviewed above address different source boundaries, including the heat sources and temperature limits considered, and different recovery objectives. In contrast, the present work combines the targeting of three exhaust streams as one source with a comparison, on a common basis, of subcritical and supercritical organic cycles and a steam reference cycle whose working-fluid heating curves are placed against that source.

The preheater exit gas carries false air, the ambient air that leaks into the preheater through the tower and the feed system. The cement literature quantifies false air from the oxygen rise across the tower and accounts for it as a fuel and fan power penalty [32]. More recently, the air ingress of cement plants has been shown to raise the cost of retrofitted membrane CO_2 capture [35]. However, false air also changes the exhaust as a heat source. The leakage cools the preheater exit gas by mixing and enlarges its mass flow, and the recoverable heat of the stream depends on both its temperature and its mass flow. Whether sealing the tower raises or lowers the heat that a recovery cycle can take from the gas therefore depends on the temperature enthalpy profile of the gas after sealing. The fuel accounting of false air does not answer this question.

Among the cement studies reviewed here, three features have not been combined in one analysis. First, the studies that set heat recovery targets by pinch analysis use modeled streams [27] or the existing network of a single waste-heat plant [28], and the studies built on measured plant heat balances place cycles on one or two of the exhaust streams. The three exhaust streams of a line with a measured heat balance have not been targeted together as one source subject to the process constraints of that line. Second, false air has been treated as a fuel and fan power penalty [32] and, more recently, as a cost variable of downstream carbon capture [35], but not as a variable of the recoverable heat and power target. Third, recent comparisons on a common basis include subcritical, supercritical and zeotropic mixture cycles on prescribed heat sources [12] and pure fluids and zeotropic mixtures on a single cement exhaust stream whose heat is supplied through an oil loop [16,17], but not on the composite curve of the measured streams of a cement line. Therefore, the location at which the heating profile of each working fluid reaches its limiting approach on such a source has not been identified in these studies.

These gaps motivate the present work, which takes as its source the three exhaust streams of a dry-process cement line described by its measured heat balance: the preheater exit gas, the bypass gas after its quench and the cooler exhaust. Its objective is threefold. The first is to determine the pinch-constrained heat and net power targets of these streams. The second is to compare, under the same thermal constraints, six cycles placed on the

composite curve of these streams: four recuperated subcritical organic cycles with toluene, cyclohexane, a toluene–cyclohexane mixture and an n-pentane–toluene mixture; a recuperated supercritical cyclopentane cycle; and a steam Rankine reference without recuperation. The third is to quantify the effects of the exit limits of the streams, which are their minimum allowable exit temperatures, of the raw mill, whose operation raises the exit limit of the preheater gas, and of the removal of the excess false air (Section 2). The targets are obtained at these exit limits, with the raw mill running and stopped and at minimum approaches of 5, 10 and 20 K in the source exchangers. The excess false air is taken out of the preheater exit stream by a species-conserving mixing balance, and the effect of its removal is evaluated as the difference between the targets with and without it: in the fixed designs, with the measurement uncertainty propagated into that difference, and nominally after the cycles are reoptimized. The contributions are:

- The heat, exergy and net power targets of the three exhaust streams of a cement line described by its measured heat balance, obtained by pinch analysis with the process exit limits and the raw mill modes of the line;
- The fractions of the composite heat targets reached with a series arrangement and with a parallel preheating arrangement of the three source exchangers, and how closely the targets are approached with an idealized two-section split-flow arrangement;
- The placement of the profiles of pure organic fluids evaporating at a constant temperature, zeotropic mixtures and a supercritical fluid, and of steam, on the composite curve of the measured source, with the location and value of the limiting approach of each profile identified and the source-exchanger exergy destruction reported beside the net power;
- The effect of removing the excess false air of the preheater on the recovery target, evaluated by a species-conserving mixing balance, with the measurement uncertainty propagated into the difference between the targets with and without that air at the fixed designs;
- The propagation into the heat and power targets of the measurement bounds adopted for the inputs taken from the plant balance.

Section 2 describes the line and its measured streams, Section 3 the method and Section 4 its validation against published results. Section 5 presents the results, and Section 6 draws the conclusions.

2. System Description

The study is configured for the exhaust streams of a dry-process cement line. In its preheater, two parallel strings of five cyclone stages each, the raw meal is heated by the rising hot gas, and it is largely calcined in an in-line calciner, a combustion vessel between the preheater and the rotary kiln. The clinker leaving the kiln is cooled by ambient air in a grate cooler. A kiln gas bypass extracts part of the kiln gas at the kiln inlet and cools it with quench air. Three streams leave the line above the temperature at which heat recovery is practicable: the preheater exit gas (A), the bypass gas after its quench (B) and the cooler exhaust air (C), as marked in Figure 1. These three streams are the heat source of the cycles placed against them by pinch-point analysis [18,19]: recuperated organic Rankine cycles with subcritical and supercritical working fluids and a steam Rankine reference cycle without a recuperator. In the source exchangers, each cycle is represented by the heating profile of its working fluid, and its state points are defined in Section 3.

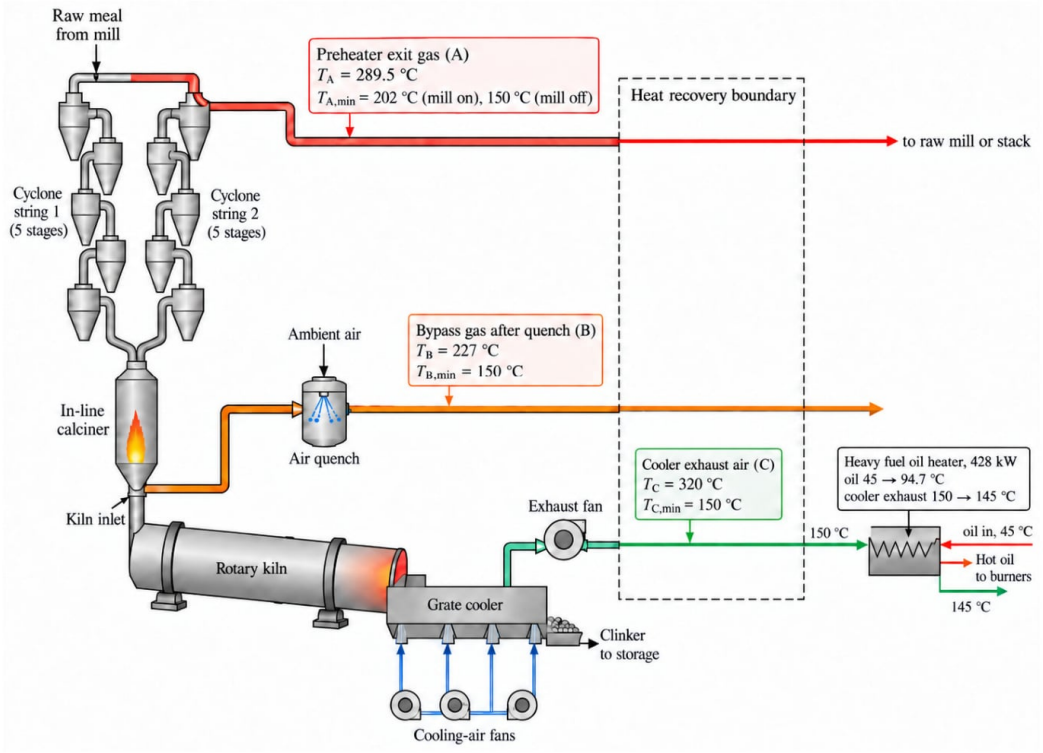

Figure 1. Gas paths of the cement line and the three exhaust streams, A, B and C.

The operating point was taken from a heat balance survey of the line made at the site. The survey report combines site measurements of the gas flows, temperatures and gas compositions with the control-room operating records and the laboratory analyses. The duct flows were calculated from the dynamic pressures measured with Pitot tubes, which give the gas velocity, together with the tube coefficients, the gas densities and the duct areas. The gas analyzer readings are recorded in the report at the kiln inlet, the two preheater string outlets, the calciner outlets and the bypass outlet. As a consistency check on these measurements, the specific heat consumption obtained from them differs by 0.33% from the control-room estimate based on the oil counter.

All stream conditions, operating parameters and integration constraints are summarized in Table 1. The basis of each value is marked by a superscript in the table: M for a measured or reported plant input, D for a value derived from the measurements and A for an adopted constraint. Volumes are given at the normal conditions of 0 °C and 101.325 kPa on a wet basis, which includes water vapor, and compositions and oxygen readings on a dry basis, which excludes it. The stream flows, temperatures and compositions are the measured values of the plant heat balance of the line at a clinker production of 183 t/h and a specific heat consumption of 883 kcal/kg of clinker. For the pyroprocessing circuit, the preheater, calciner, kiln and cooler through which the gases pass, the report gives a gas balance discrepancy of 0.7%. The moisture of the preheater exit gas and the bypass gas follows from their measured dry and wet normal densities. The mass flows and specific heats then follow from the normal volume flows and the compositions by the relations of Section 3.2. Above the 33 °C ambient, the preheater exit gas carries 28.3 MW, the bypass gas 23.3 MW and the cooler exhaust 24.7 MW, or 133, 109 and 116 kcal/kg of clinker, respectively. These values agree within 2% with those of the plant balance, which are evaluated above a reference temperature that the report does not state.

Table 1. Stream conditions, operating parameters and integration constraints.

Category	Parameter	Symbol	Value	Unit
Plant operating point	Clinker production [M]	$\dot{m}_{cl}$	183	t/h
	Kiln feed [M]	$\dot{m}_{kf}$	320	t/h
	Specific heat consumption [M]	SHC	883	kcal/kg cl
	Bypass rate [M]	—	29.8	%
	Ambient temperature [M]	T_{amb}	33	°C
Preheater exit gas (A)	Volume flow [M]	$\dot{V}_A$	259,864	Nm^3/h
	Temperature [M]	T_A	289.5	°C
	Dry composition $O_2/CO_2/N_2/CO$ [M]	y_i	4.2/37.6/58.2/0.015	vol%
	Dry/wet normal density [M]	ρ_{dry}/ρ_{wet}	1.5245/1.496	kg/Nm^3
	Moisture [D]	x_w	3.96	vol%
	Mass flow [D]	$\dot{m}_A$	108.0	kg/s
	Dust load [M]	—	16.5	t/h
	Minimum exit temperature, mill on/mill off [A]	$T_{A,min}$	202/150	°C
Bypass gas after quench (B)	Volume flow [M]	$\dot{V}_B$	322,199	Nm^3/h
	Temperature [M]	T_B	227	°C
	Dry composition $O_2/CO_2/N_2/CO$ [M]	y_i	19.2/3.2/77.6/0.0018	vol%
	Dry/wet normal density [M]	ρ_{dry}/ρ_{wet}	1.306/1.286	kg/Nm^3
	Moisture [D]	x_w	4.0	vol%
	Mass flow [D]	$\dot{m}_B$	115.1	kg/s
	Dust load [M]	—	5.5	t/h
	Minimum exit temperature [A]	$T_{B,min}$	150	°C
Cooler exhaust air (C)	Volume flow [M]	$\dot{V}_C$	232,356	Nm^3/h
	Temperature [M]	T_C	320	°C
	Composition [A]	—	air	—
	Mass flow [D]	$\dot{m}_C$	83.5	kg/s
	Minimum exit temperature [A]	$T_{C,min}$	150	°C
Process cold stream	Heavy fuel oil flow [M]	$\dot{m}_{HFO}$	16.3	t/h
	Inlet temperature [A]	$T_{HFO,in}$	45	°C
	Outlet temperature [M]	$T_{HFO,out}$	94.7	°C
	Duty [D]	$\dot{Q}_{HFO}$	428	kW
False air, preheater	Outlet volume flow, string 1/string 2 [M]	—	129,944/129,920	Nm^3/h
	O_2 at calciner cyclone/string outlet, string 1 [M]	—	0.53/4.50	vol% dry
	O_2 at calciner cyclone/string outlet, string 2 [M]	—	0.37/3.96	vol% dry
	False air fraction of the inlet gas (from the O_2 rise) [D]	—	22.6	%
	Airlift blower air (metered) [M]	$\dot{V}_{al}$	27,835	Nm^3/h
	Removable excess, consistent basis (this study) [D]	$\dot{V}_{fa}$	5983	Nm^3/h
	Removable excess, plant accounting [D]	$\dot{V}_{fa,plant}$	15,210	Nm^3/h
Cooling water	Inlet/outlet temperature [A]	T_{cw}	30/35	°C
	Approach in the condenser [A]	ΔT_{cond}	5	K
Heat recovery integration	Minimum approach in the source exchangers [A]	ΔT_{min}	5 (10, 20)	K
	Dead-state temperature [A]	T_0	25	°C

The minimum allowable exit temperature of each stream, its exit limit, determines how much of the measured stream heat the source exchangers that supply the cycle can recover. The preheater gas is the drying medium of the raw mill, so its exit limit is 202 °C when the mill runs and 150 °C when it does not. The bypass gas carries the alkali- and chloride-enriched dust that the bypass exists to remove, and a higher exit limit of 180 °C is

examined for it as a sensitivity case (Section 3.10). In the base case of the study, the raw mill is stopped and the minimum approach in the source exchangers is 5 K, and the three streams have a common exit limit of 150 °C, the recovery cutoff adopted for them. For the two combustion gas streams, the preheater exit gas and the bypass gas, this cutoff is motivated by the risk of acid condensation. Within the recovery boundary of this study, the line has one process cold stream: the heating of the heavy fuel oil (HFO) to 94.7 °C before the burners, a duty of 428 kW. This duty is served from the cooler exhaust below its exit limit, as Section 3.4 shows.

The plant balance also quantified the false air entering the preheater from the rise in oxygen across the tower: the false air amounts to 22.6% of the gas entering the tower. The four airlift blowers that convey the kiln feed to the tower account for 27,835 Nm^3/h of that air, and the plant sets 6% as the acceptable leakage. When the percentages are taken on the gas entering the tower, a basis termed here the consistent basis, the excess above that level is 5983 Nm^3/h. The plant's own accounting applies them to the exit flow, a basis termed here the plant accounting basis, and gives 15,210 Nm^3/h. Both quantities are carried in Table 1 and used in Section 3.9, where the excess is removed from the preheater exit stream to obtain its effect on the recoverable power. In the cement literature, false air is treated as a fuel and fan power penalty [32]. Here, in contrast, its effect on the exhaust as a heat source is examined.

3. Methodology

The model combines pinch analysis with steady-state cycle calculations, in the manner of pinch-based ORC design studies [20–22]. The source streams are combined into composite and grand composite curves that set the heat targets and the placement condition. A steady-state cycle model then converts the heat target of each cycle into a power target. The mixture calculations account for composition and temperature glide, and a mixing balance modifies the preheater stream for the false air case. The numerical settings are collected in Table 2.

3.1. Assumptions

The following assumptions are adopted in the model, each applied in the subsection indicated:

1. The line operates at steady state at the measured operating point of the plant balance, and the three exhaust streams are ideal gas mixtures at atmospheric pressure with temperature-dependent heat capacities (Section 3.2).
2. The streams are combined only in the composite curve, and no physical mixing of the gases takes place (Section 3.4).
3. Each stream is cooled in the source exchangers no lower than its exit limit, and the heating of the fuel oil is supplied by the cooler exhaust below its cutoff, outside the source cascade (Sections 3.3 and 3.4).
4. The minimum approach in the source exchangers is 5 K in the base case and 10 and 20 K in the sensitivities, and no pressure drop is taken on either side of any exchanger, except for the working-fluid pressure drop of the sensitivity analysis (Sections 3.6 and 3.10).
5. The sensible heat of entrained dust is excluded from the recovery targets, except in the sensitivity case with the dust included, and fouling is not modeled (Sections 3.2 and 3.10).
6. The cycle is at steady state, with isentropic efficiencies of 0.85 for the turbine and 0.65 for the pump, and the condenser delivers saturated liquid at 40 °C against cooling water heated from 30 to 35 °C, except in the sensitivity cases in which the condensing pressure, the cooling-water temperature rise or the component efficiencies are varied (Sections 3.7 and 3.10).

7. The recuperator cold-end approach is 5 K, the working fluid of the subcritical organic cycles enters the turbine with 0.1 K of superheat, and no generator, fan or auxiliary losses are taken (Section 3.7).
8. Working-fluid properties follow the Helmholtz energy equations of state with the fitted binary interaction parameters, and subcooled-mixture liquid states are taken from the saturated liquid with the pressure corrections (Section 3.7).
9. False air enters the preheater at the ambient temperature and is removed by a species-conserving mixing balance, the plant's 6% allowance defining the removable excess (Section 3.9).
10. The input uncertainties are evaluated by the Type B method, from bounds adopted for the measurement types rather than from the scatter of repeated readings, with independent rectangular distributions for the individual readings (Section 3.10).

3.2. Stream Properties and Heat Availability

The moisture content of each gas stream is obtained from the dry and wet normal densities recorded at the measuring points,

$$x_w = \frac{\rho_{dry} - \rho_{wet}}{\rho_{dry} - \rho_w} \tag{1}$$

where ρ_{dry} and ρ_{wet} are the normal densities of the dry and wet gas and $\rho_{\mathrm{w}} = 0.804\ \mathrm{kg/Nm^3}$ is the normal density of water vapor. Equation (1) gives 3.96% by volume for the preheater exit gas and 4.0% for the bypass gas; the cooler exhaust is air. The wet composition follows from the dry analyzer readings scaled by $(1 - x_{\mathrm{w}})$.

The specific heat of the wet mixture at any temperature is the mole weighted ideal gas value [36],

$$c_p(T) = \frac{\sum_i y_i \bar{c}_{p,i}(T)}{\sum_i y_i M_i} \tag{2}$$

where y_{i} is the mole fraction, M_{i} the molar mass, and $\bar{c}_{p,i}$ the molar isobaric heat capacity of CO_2, N_2, O_2, CO and H_2O. The heat capacities are evaluated with the CoolProp library, version 8.0.0 [37], in the ideal gas limit, since the streams are at atmospheric pressure. At 289.5 °C, the CO_2 rich preheater gas has $c_{\mathrm{p}} = 1.078\ \mathrm{kJ/(kg\ K)}$, 7% above the constant $1.005\ \mathrm{kJ/(kg\ K)}$ of the plant balance.

The mass flow of each stream is $\dot{m}_{\mathrm{s}} = \dot{V}_{\mathrm{s}}\rho_{\mathrm{wet}}/3600$, the product of its normal volume flow and its wet normal density, with the factor 3600 converting the flow per hour to flow per second. The stream data of pinch analysis [18] give the heat that a stream releases in cooling from its supply temperature, T_{s}, to a temperature, T, above its exit limit, T_{f}, the integral of its heat capacity flow rate over that cooling range,

$$\dot{Q}_s(T) = \dot{m}_s \int_{\max(T,\,T_f)}^{T_s} c_p(T')\,dT' \quad (T < T_s), \qquad \dot{Q}_s(T) = 0 \quad (T \geq T_s) \tag{3}$$

where $\dot{m}_{\mathrm{s}}$ is the stream mass flow. The integral is evaluated by numerical quadrature, and a stream contributes nothing above its supply temperature. The heat above the ambient reported in Section 2 is obtained using Equation (3), evaluated with the ambient temperature as its lower limit, and the mean heat capacity flow rate of a stream is that heat divided by $(T_{\mathrm{s}} - T_{\mathrm{amb}})$. In the sensitivity case with the entrained dust included, the capacity rate of the preheater and bypass streams is increased by that of their dust, carried at the gas temperature. Equation (3) is then evaluated with $\dot{m}_{\mathrm{s}}c_{\mathrm{p,s}} + \dot{m}_{\mathrm{d,s}}c_{\mathrm{p,d}}$ in place of $\dot{m}_{\mathrm{s}}c_{\mathrm{p,s}}$, where $\dot{m}_{\mathrm{d,s}}$ is the dust mass flow of stream s and $c_{\mathrm{p,d}}$ the dust specific heat (Table 2).

3.3. Exit-Temperature Limits

Each stream is assigned an exit temperature below which the source exchangers of the cycles take no heat from it. Because the preheater gas is the drying medium of the raw mill (Section 2), two operating modes are carried through the analysis. In the mill-on mode, with the raw mill running, the exit limit of the preheater gas is 202 °C (Table 1). In the mill-off mode, it is 150 °C, and neither the preheater exit gas nor the bypass gas is cooled below this limit in any case of the study. The cooler exhaust is represented as air, with no acid dew point constraint imposed in the model. Its base-case recovery cutoff is set at 150 °C, which is consistent with the practical cooler exhaust outlet temperatures of 140–150 °C reported in cement-plant waste-heat recovery studies [2,38]. The effect of reducing this cutoff to 100 °C is examined in the cooler floor case of Section 3.10. The bypass gas, with its chloride- and potassium-enriched dust [5], has a limit of 150 °C in the base case and 180 °C in the bypass floor case of Section 3.10.

3.4. Composite Curves and the Grand Composite Curve

The recoverable heat of the line is represented by the hot composite curve of pinch analysis [18,39], the sum over the three streams of Equation (3) at each temperature,

$$H(T) = \sum_{s} \dot{Q}_s(T) \tag{4}$$

which gives the heat released by the streams together above any temperature, T, between the lowest exit limit and the highest supply temperature. The composite is a sum of the stream heat curves and does not represent a physical mixing of the gases.

The targets are obtained by the problem table algorithm of Linnhoff and Flower [39] in the form given by Kemp [18]. Hot stream temperatures are shifted down by half the minimum approach,

$$T^* = T - 1/2\Delta T_{min} \tag{5}$$

where ΔT_{min} is the minimum temperature approach between the source and the working fluid. The shifted supply and exit temperatures of the streams define the temperature intervals, in each of which the net heat is

$$\Delta H_k = \sum_{h} \dot{Q}_{h,k} \tag{6}$$

where $\dot{Q}_{h,k}$ is the heat released by stream h within interval k from Equation (3). The net heats are cascaded from the highest interval downward,

$$R_k = R_{k-1} + \Delta H_k, \qquad R_0 = 0 \tag{7}$$

where R_{k} is the heat passed from interval k to the next lower interval and R_{N}, its value below the lowest interval, is the heat that an external sink, the cold utility, would have to remove. The grand composite curve (GCC) is R_{k} plotted against shifted temperature. The cascade of the three exhaust streams is a surplus-only cascade, one in which every interval releases heat and none requires it. The pinch therefore lies at the top of the cascade, and no hot utility, heat supplied from an external source, is required; the cold utility target, R_{N}, is the whole surplus above the exit limits. This is the threshold case of pinch analysis, in which one utility requirement vanishes [18], and the target is the heat available for cycle heat recovery. Because the analysis targets the selected exhaust streams rather than all hot and cold streams of the plant, the absence of a hot utility applies to this recovery boundary. The one process cold stream within this boundary, the fuel oil heating of 428 kW, is matched separately by the cooler exhaust below its exit limit. Supplying this duty cools the cooler exhaust from 150 to 145.0 °C in the base case, and that segment is counted once and never enters the source cascade.

3.5. Exergy of the Source

The quality of the surplus is measured by its thermal exergy relative to an adopted dead state, T_0, of 25 °C, the reference environment of the exergy method [36,40],

$$\dot{E}_{src} = \sum_{s} \dot{m}_s \int_{T_{out,s}}^{T_s} c_p(T)\left(1 - \frac{T_0}{T}\right) dT \tag{8}$$

with temperatures in kelvin [36], where $T_{\mathrm{out,s}}$ is the temperature at which stream s actually leaves the source exchangers. Equation (8) evaluated down to the exit limits is the ceiling on the shaft power that any heat engine placed on the source can approach. Evaluated down to the actual outlets, it is the thermal exergy decrease of the source streams, of which the working fluid takes up the part given by Equation (19).

3.6. Placement of the Heat Engine on the Source

Townsend and Linnhoff [19] stated the appropriate placement principle: a heat engine is placed entirely on one side of the process pinch, so that it takes no heat across the pinch. Below the pinch, it acts as a cold utility, and its heating profile, shifted up by half the minimum approach, must lie under the grand composite curve. For the selected exhaust streams, the whole surplus lies below the pinch, and the cascade contains only the three hot streams, so the grand composite curve is the hot composite curve of Equation (4) shifted down by half the minimum approach. The cycle is therefore placed against the hot composite curve directly, and the minimum approach is evaluated on actual temperatures using Equation (9).

At a given pressure and composition, the bubble and dew temperatures mark the beginning and the completion of evaporation, respectively. The working-fluid heating profile runs from the temperature at which the fluid enters the source exchangers to the turbine inlet. The heat coordinate of the placement starts at the hot end, where the composite is at its highest temperature and the fluid at its turbine inlet; the figures of Section 5 plot the heat from the cold end. The fluid mass flow is the largest value for which the profile keeps the minimum approach everywhere. Following the appropriate placement principle [19] and source-constrained ORC design [20], this study imposes the following pointwise minimum approach condition, Equation (9):

$$\dot{m}_{wf} = \max\left\{\dot{m} : \; T_{hot}(q) - T_{wf}(q) \geq \Delta T_{min} \quad \forall\, q \in [0,\, \dot{m}\, q_{in}]\right\} \tag{9}$$

where q is the heat counted from the hot end of the composite curve, $T_{\mathrm{hot}}(q)$ the composite temperature at that heat, $T_{\mathrm{wf}}(q)$ the fluid temperature at the corresponding enthalpy, and q_{in} the heat taken by one kilogram of fluid. The checkpoints include the breakpoints of the composite, where its slope changes at the supply temperatures and exit limits of the streams, and the bubble and dew points of the fluid, so the condition is tested where the approach is smallest. The limiting location is where the temperature difference is smallest; when the approach constraint is active, this minimum equals ΔT_{min}. Section 5.2 reports the locations for the retained base designs.

When the fluid absorbs the whole surplus at the minimum approach, every stream is cooled to its exit limit. Otherwise, the streams are cooled to a common outlet temperature or to their limits, whichever is higher,

$$T_{out,s} = \max\left[T_{hot}\left(\dot{m}_{wf}\, q_{in}\right),\; T_{f,s}\right] \tag{10}$$

which is the allocation of heat between streams that the composite curve implies. The composite targets are obtained on the assumption that the hotter streams can serve more than one section of the working-fluid heating curve, as required by vertical matching, in which each section of the heating curve takes its heat from the part of the composite

directly above it in the temperature–heat diagram. Therefore, the targets are reported as upper bounds on the recovery a network realizes [18,25], and Section 5.3 compares three arrangements of the source exchangers with the composite targets. The design variables of the placement are the bubble temperature for the subcritical organic cycles, the turbine inlet temperature for supercritical cyclopentane, and the drum pressure and superheat for steam. They are searched for each cycle to the values that maximize the net power target, and the design with the highest net power within the declared search domain in Table 2, for steam, its adopted superheat range of 1 to 120 K, is termed the retained design.

Three arrangements of the source exchangers are defined for the comparison of Section 5.3. In the series arrangement, the working fluid passes through the three source exchangers in sequence, taking heat first from the coolest stream, the bypass gas, then from the preheater exit gas and last from the hottest, the cooler exhaust. In the parallel preheating arrangement, the fluid flow is divided between two preheating exchangers, on the cooler exhaust and on the bypass gas, and the recombined flow is then heated by the preheater gas. In the idealized two-section split-flow arrangement, the fluid first passes a lower section of three parallel exchangers, one on each stream, and then an upper section of two parallel exchangers, on the preheater exit gas and the cooler exhaust; the branches of each section recombine at its outlet. These two streams pass their upper exchanger first and then their lower one. In the split-flow arrangement of the steam cycle, a superheater on the cooler exhaust follows the upper section and takes the whole steam flow, and the cooler exhaust passes it before its upper exchanger. In every arrangement, each stream is cooled in counterflow no lower than its exit limit, the approach is checked along each exchanger, and the fluid outlet enthalpy of each stage is the largest that the stream can deliver. For stage j, the exchanger on one stream, the energy balance is

$$z_j \dot{m}_{wf}\left(h_{j,out} - h_{j,in}\right) = \dot{m}_{s,j}\int_{T_{out,j}}^{T_{in,j}} c_p \, dT, \qquad T_{out,j} \geq T_{f,j}, \quad T_s(q) - T_{wf}(q) \geq \Delta T_{min} \tag{11}$$

where $h_{\mathrm{j,in}}$ and $h_{\mathrm{j,out}}$ are the fluid enthalpies at the inlet and outlet of the stage, z_{j} is the fraction of the working-fluid mass flow passing it, and $T_{\mathrm{in,j}}$ and $T_{\mathrm{out,j}}$ are the stream inlet and outlet temperatures. The largest fluid outlet enthalpy that satisfies both the exit limit and the minimum approach of Equation (11) is retained, and the outlet of one stage is the inlet of the next. In the series arrangement, $z_{\mathrm{j}} = 1$. In a split arrangement, a section of the heating curve is shared between parallel stages, with $\Sigma z_{\mathrm{j}} = 1$ within the section and all stages of the section leaving at the same fluid state. A stream passing two stages enters the second at the outlet temperature of the first.

The three arrangements are applied to the retained design of each cycle on two bases. On the heat basis, used for the series and parallel preheating arrangements, the working fluid keeps the retained mass flow, that of the composite target, and the fraction of the composite heat target that it absorbs is reported in Section 5.3. On the operating point basis, used for the series and split-flow arrangements, the cycle states and efficiencies of the retained design are held, and the working-fluid mass flow is the highest at which the fluid still reaches the retained turbine inlet state in the arrangement. For the split-flow arrangement, this mass flow is found by a search over the boundary between the lower and upper sections and over the mass flow fractions of the branches; the series arrangement has no boundary or fractions to search. The net power follows from Equation (18). The search finds a feasible allocation, not an optimal network. As in the placement, the approach is checked at every node of the fluid and gas curves, sampled at the settings in Table 2. Where the fluid does not reach the retained inlet state in an arrangement at the retained mass flow, the composite net power target remains an upper bound for that arrangement.

3.7. Cycle Model

The cycle model converts the heat target into a power target by steady-state energy balances on each component [6,36], with the notation of Figure 2 and the fixed parameters in Table 2. The working fluid leaves the condenser as a liquid at state 1 and is pumped to state 2. In the organic cycles, the recuperator preheats it to state 3, at which point it enters the source exchangers. It is heated there to the turbine inlet state 4 and expanded in the turbine to state 5. The turbine exhaust is cooled in the recuperator to state 6 and condensed back to state 1. The steam cycle has no recuperator, so its state 3 coincides with state 2, and the steam expands in the turbine from state 4 to state 5 and is condensed from there.

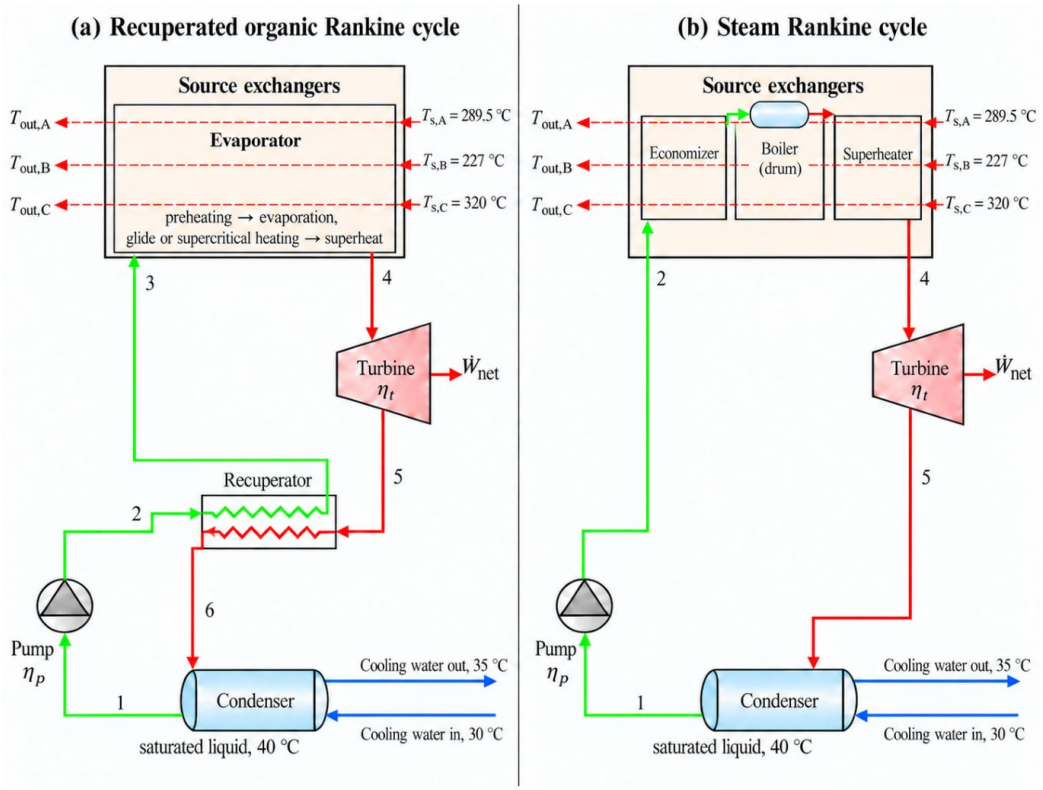

Figure 2. Schematics and state points of (**a**) the recuperated organic Rankine cycle and (**b**) the steam Rankine cycle.

The fluid leaves the condenser as a saturated liquid at its bubble point, $T_1 = 40$ °C. Cooling-water temperatures of 30 °C at inlet and 35 °C at outlet, together with a 5 K minimum approach, are adopted. The approach is verified along the whole condensation path by Equation (21). The pump raises the liquid to the operating pressure of the cycle,

$$h_2 = h_1 + \frac{h_{2s} - h_1}{\eta_p} \tag{12}$$

where h_{2s} is the isentropic outlet enthalpy and $\eta_p = 0.65$ is the pump isentropic efficiency.

For the organic fluids, which are dry, the pumped liquid is preheated in a recuperator by the turbine exhaust, the internal heat recovery used with dry fluids in ORC practice [41,42]. The recuperator is specified by its cold-end approach,

$$T_6 = T_2 + \Delta T_{rec} \tag{13}$$

$$h_3 = h_2 + (h_5 - h_6) \tag{14}$$

where $\Delta T_{rec} = 5$ K. Three limits apply to Equation (14),

$$T_5 - T_3 \geq 5\,\text{K}, \qquad T_3 \leq T_{bubble}(p_{evap}) - 2\,\text{K}, \qquad T_6 \geq T_{dew}(p_{cond}) + 1\,\text{K} \tag{15}$$

the hot-end approach, which keeps the turbine exhaust at least 5 K above the preheated liquid; the liquid outlet at least 2 K below the bubble temperature at the evaporation pressure for the subcritical organic cycles, so that evaporation begins in the source exchangers and not in the recuperator; and the vapor outlet at least 1 K above its dew point, so that the exhaust does not begin to condense in the recuperator. At the supercritical pressure, no bubble point exists, and only the hot-end and vapor outlet limits apply. When a limit binds, the liquid outlet is set by the limit and the vapor outlet follows from the balance; when the turbine exhaust is too cold to preheat the pumped liquid, the recuperator is bypassed. The approach inside the recuperator is checked at 20 equally spaced points along the enthalpy balance, not at its ends only. When the 48 retained organic designs of the base, operating and constraint cases (Section 3.10) and the 19 designs of the composition and pressure sensitivity were rechecked at 40 and 80 points, the minimum internal approach was the same as at 20 points.

The fluid takes its heat from the source between states 3 and 4,

$$q_{in} = h_4 - h_3 \tag{16}$$

and the turbine inlet state 4 is the dew point plus an adopted 0.1 K of superheat for the subcritical organic cycles. A near-saturated inlet suffices for these dry fluids, since their expansion from saturated vapor ends in the superheated region and no liquid forms in the turbine. For the supercritical cycle, state 4 is set by the pressure and the turbine inlet temperature, and for steam by the drum pressure and the superheat. The steam superheat is searched over the adopted 1 to 120 K domain, and the design found there is the steam reference. The search is also extended at each drum pressure up to the superheat limit set by the source, $\Delta T_{\mathrm{sh,max}} = T_{\mathrm{s,max}} - \Delta T_{\mathrm{min}} - T_{\mathrm{sat}}(p_{\mathrm{evap}})$, at which the turbine inlet temperature reaches the prescribed approach to the hottest stream. The design found in this extended search is reported beside the reference (Sections 5.2 and 5.6). The steam outlet quality, x_5, the vapor mass fraction at the turbine exit, is held at or above 0.88 to limit the exhaust wetness that erodes turbine blading. The expansion is

$$h_5 = h_4 - \eta_t(h_4 - h_{5s}) \tag{17}$$

where h_{5s} is the isentropic outlet enthalpy and $\eta_{\mathrm{t}} = 0.85$ is the turbine isentropic efficiency. The net power target and the exergy taken up by the fluid are

$$\dot{W}_{net} = \dot{m}_{wf}[(h_4 - h_5) - (h_2 - h_1)] \tag{18}$$

$$\dot{E}_{wf} = \dot{m}_{wf}[(h_4 - h_3) - T_0(s_4 - s_3)] \tag{19}$$

and the exergy destroyed in the source exchangers is

$$\dot{E}_D = \dot{E}_{src} - \dot{E}_{wf} \tag{20}$$

with $\dot{E}_{\mathrm{src}}$ from Equation (8) evaluated down to the actual outlets of Equation (10). Source-exchanger exergy destruction is the second law measure used for the temperature match between a source and a working-fluid profile [10,43]. It is reported beside the net power, which measures the performance of the complete cycle. The net power is the turbine power less the pump power, without generator, fan or auxiliary losses. The thermal efficiency is $\eta_{\mathrm{th}} = \dot{W}_{\mathrm{net}}/(\dot{m}_{\mathrm{wf}}\, q_{\mathrm{in}})$. The second law efficiency $\eta_{\mathrm{II}} = \dot{W}_{\mathrm{net}}/\dot{E}_{\mathrm{src}}$ and the conversion efficiency $\eta_{\mathrm{conv}} = \dot{W}_{\mathrm{net}}/\dot{E}_{\mathrm{wf}}$ are rational efficiencies in the sense of Kotas [40], the net power over the exergy input of a control volume. For η_{II}, the control volume is the source exchangers together with the cycle, with $\dot{E}_{\mathrm{src}}$ of Equation (8) evaluated down to the actual stream outlets; for η_{conv}, it is the cycle alone, with $\dot{E}_{\mathrm{wf}}$ of Equation (19).

The condensation of each design is checked along the condenser at constant pressure, from its actual inlet state to the saturated liquid outlet (state 1). The inlet state is the recuperator outlet (state 6) for the organic cycles and the wet turbine exit (state 5) for steam. The cooling water rises in counterflow over the total heat rejection duty, and the condition is

$$T_{wf}(q_c) - \left[T_{cw,in} + \left(T_{cw,out} - T_{cw,in} \right) \frac{q_c}{q_{cond}} \right] \geq \Delta T_{cond} \quad \forall\, q_c \in [0,\, q_{cond}] \tag{21}$$

where q_c is the heat rejected per kilogram of fluid counted from the liquid outlet and $T_{wf}(q_c)$ the fluid temperature along the condensation path. The heat rejected per kilogram of fluid in the condenser, q_{cond}, is $h_6 - h_1$ for the organic cycles and $h_5 - h_1$ for steam. $T_{cw,in}$ and $T_{cw,out}$ are the cooling-water inlet and outlet temperatures, between which the water temperature rises linearly with the duty in counterflow, and ΔT_{cond} is the prescribed condenser approach (Table 2). The condensation paths are evaluated for the six base designs and for the 52 designs of the sensitivity analysis. For the other operating cases of the study, the modeled path lies at or above the 40 °C outlet, while the water lies between 30 and 35 °C, so the local difference cannot fall below 5 K. Each path is evaluated at 400 points of the duty with local refinement about the minimum, on a property path that includes the bubble and dew states of the mixtures; doubling the resolution changes the minimum approaches by less than 0.0001 K. These checks establish the feasibility of each design at the prescribed 40 °C outlet under common cooling conditions; they are not an optimization of the condenser for each fluid.

The volume flow ratio (VFR) across the turbine, the ratio of the outlet to the inlet specific volume,

$$VFR = \frac{v_5}{v_4} \tag{22}$$

is reported for every placed design against a VFR of 50, adopted as the screening threshold for single-stage expansion following Shu et al. [8]. The isentropic form of this ratio is a similarity parameter of turbine efficiency, as established by Macchi and Perdichizzi [44]. The threshold is not imposed in the base comparison, because the study sets targets for the source and does not design the turbine; designs above it are flagged for further expander assessment, including multistage expansion, and Section 3.10 adds a case in which VFR $\leq$ 50 is imposed. The threshold is a screen for the organic expanders, and steam is reported on the same basis for comparison. The evaporation pressure of the subcritical organic cycles is limited to 90% of the critical pressure, following Zhai et al. [45], and the turbine inlet temperature of every organic working fluid to the thermal stability limit of Section 3.8. For the mixtures, an adopted screening pressure replaces the critical pressure in the first limit: 0.9 × 40.5 bar for toluene–cyclohexane, where 40.5 bar is an adopted reference below the 40.8 bar critical pressure of cyclohexane, and 0.9 × 33.7 bar for n-pentane–toluene, where 33.7 bar is the critical pressure of n-pentane.

Table 2. Fixed parameters and numerical settings of the placement and the cycle model.

Parameter	Symbol	Value	Basis
Minimum approach in the source exchangers	ΔT_{min}	5 (10, 20) K	Adopted targeting basis and sensitivity values
Condensation, bubble point	T_1	40 °C	Adopted cooling water 30 → 35 °C; 5 K approach
Pump isentropic efficiency	η_p	0.65	Adopted

Table 2. *Cont.*

Parameter	Symbol	Value	Basis
Turbine isentropic efficiency	η_t	0.85	Fixed efficiency precedent [46]
Recuperator cold-end approach	ΔT_{rec}	5 K	Adopted
Superheat, subcritical organic cycles	—	0.1 K	Adopted; dry fluids
Evaporation pressure limit, subcritical	$p_{evap} \leq 0.9\, p_{crit}$	Mixtures: 0.9 × 40.5 bar (toluene–cyclohexane) and 0.9 × 33.7 bar (n-pentane–toluene)	Zhai et al. [45]; adopted screening limits for the mixtures (Section 3.7)
Supercritical pressure	$p = 1.25\, p_{crit}$	57.3 bar	Section 3.8
Dead-state temperature	T_0	25 °C	Adopted reference environment; exergy definition [36,40]
Volume flow ratio, single-stage screening threshold	VFR	50	Shu et al. [8]
Mixture compositions (fixed)	—	A: toluene–cyclohexane 50/50 by mass (0.477/0.523 mole); B: n-pentane–toluene 30/70 by mass (0.354/0.646 mole)	Section 3.8
Design search domain, subcritical organics	T_{bubble}	150 °C up to the lowest of the stability cap less 20 K, the source top less (ΔT_{min} + 1 K) and the bubble temperature at the evaporation pressure limit, which in the 5 K base case is 310.1 °C (toluene), 272.1 °C (cyclohexane), 280 °C (mixture A) and 245.7 °C (mixture B)	Stability cap 400 °C (toluene) [13] and 456 °C (cyclohexane, Section 3.8); adopted cap 300 °C (mixtures)
Design search domain, supercritical	T_4	240–300 °C at 1.25 p_{crit}	Stability cap 300 °C [14]
Design search domain, steam	p_{evap}, superheat	Drum pressure from the initial candidates and their refinement (3–40 bar); superheat 1–120 K (adopted upper bound); extended search: superheat up to $\Delta T_{sh,max}$ (Section 3.7)	Adopted
Composite grid/heat quadrature/placement checkpoints/heating curve points	—	300/120/200/40 per region	Converged to 0.01 MW and 0.05 K at twice the resolution

Table 2. *Cont.*

Parameter	Symbol	Value	Basis
Design search, bubble or turbine inlet temperature	—	Initial 10 K sweep; refinement: toluene and cyclohexane 1 K over ±9 K; mixtures 2 K over ±9 K, then 0.5 K over ±2 K; supercritical 1 K over ±9 K, then 0.25 K over ±2 K; golden section to 0.02 K for all	Off-grid checks find no better design
Design search, steam	—	initial drum pressures 5, 8, 10, 12, 15, 20, 25, 30 and 40 bar with superheat from 1 K in 10 K steps; refinement ±2 bar in 1 bar steps (down to 3 bar) and ±10 K in 1 K steps; extended search: 1 K steps over the 10 K below $\Delta T_{sh,max}$, 0.1 K over the last 1 K, and the limit, at each pressure	Off-grid checks at ±0.5 bar and ±0.5 K
Entrained dust, preheater and bypass gas	$\dot{m}_d$	16.47 and 5.49 t/h	Plant balance
Dust specific heat	$c_{p,d}$	0.963 kJ/(kg K)	Plant balance
Mixture compositions (sensitivity)	—	Toluene–cyclohexane from 90/10 to 5/95 and both pure fluids; n-pentane–toluene from 10/90 to 60/40, by mass	Section 3.10
Supercritical pressure (sensitivity)	p	1.10 and 1.40 p_{crit}	Section 3.10
Isentropic efficiencies (sensitivity)	η_t; η_p	0.80 and 0.90; 0.60 and 0.70	Section 3.10
Working-fluid pressure drop (sensitivity)	Δp	0.1 and 0.2 bar, before or after the source exchangers	Section 3.10
Condensing level (sensitivity)	p_{cond}	Lowest pressure meeting Equation (21) at the 5 K approach; mixture B also with water rises of 15 and 20 K	Section 3.10
Turbine efficiency, axial correlation (sensitivity)	η_t	One, two and three stages at optimized speed	Appendix A
Fluid and gas curve points of the arrangements	—	Every node of the sampled curves, with the composite breakpoints and the bubble and dew points	Section 3.6
Minimum approach in the condenser	ΔT_{cond}	5 K	Equation (21)

Fluid properties, pure and mixed, are evaluated with the Helmholtz energy equations of state implemented in CoolProp [37], with the fitted binary interaction parameters of the library for the two mixtures [47]. Mixture states inside the two-phase region are evaluated along the quality between the bubble and dew points. Subcooled-mixture liquid states are taken from the saturated liquid at the same temperature with the pressure corrections $v(1 - \beta T)(p - p_{\text{bubble}})$ on enthalpy and $-\beta v(p - p_{\text{bubble}})$ on entropy, where p is the liquid pressure, p_{bubble} the bubble pressure at that temperature and β the isobaric expansion coefficient. The corrections follow from the isothermal pressure derivatives $(\partial h/\partial p)_{\text{T}} = v(1 - \beta T)$ and $(\partial s/\partial p)_{\text{T}} = -\beta v$ of the Maxwell relations [36]. Both corrections are checked against the equation of state at the states of Section 4.5.

3.8. Working-Fluid Selection

The working fluids placed on the source are chosen to represent three ways of matching the composite curve and one industrial reference, steam. The three ways are the evaporation plateau of a pure fluid, the temperature glide of a zeotropic mixture and the continuous profile of a supercritical fluid. The glide is the difference between the dew and bubble temperatures at a given pressure [48,49]. Steam is a conventional working fluid of cement waste-heat recovery [1,2] and is therefore carried as the reference. The mixture compositions and the operating pressure of the supercritical cycle are prescribed for the comparison; they are not design variables of the placement. Their effect on the comparison is examined in the sensitivity analysis of Sections 3.10 and 5.6.

Seven candidate fluids were selected for screening on the basis of their precedents in the high-temperature ORC literature [6–8]: toluene, o-xylene, n-octane, octamethyltrisiloxane (MDM), cyclohexane, n-heptane and cyclopentane. n-Pentane was added as a mixture component. The seven candidates were assessed against five criteria. The first criterion is the critical temperature. For a subcritical cycle, it must stand above the intended evaporation temperature with a margin, because the evaporation pressure is limited to 90% of the critical pressure [45]. For a supercritical cycle, the screening interval adopted in this study places it 30 to 80 K below the usable source temperature. The supply temperatures of the three streams are 289.5 °C for the preheater exit gas, 227 °C for the bypass gas and 320 °C for the cooler exhaust. Together, these conditions place the useful critical temperatures between about 240 and 320 °C. The second criterion is thermal stability: the reported stability limit must exceed the highest fluid temperature in the placement by an adopted margin of 20 K. The third is the availability of validated properties, a multiparameter equation of state for a pure fluid and fitted binary interaction parameters for a mixture. The fourth is dry or isentropic working-fluid behavior, which allows the turbine exhaust to be superheated and to feed the recuperator. The fifth is environmental acceptability, which requires zero ozone depletion potential and negligible global warming potential. In addition to these criteria, the flammability classifications of the fluids are reported in Table 3.

Toluene satisfies all five criteria and is a reference fluid in high-temperature ORC studies [7]. Its critical temperature of 318.6 °C is close to the supply temperature of the cooler exhaust, the hottest stream. Invernizzi et al. report that toluene is stable up to about 400 °C [13,50], and it is dry. Its disadvantage is the condensing pressure of 0.079 bar at 40 °C and the large volume flow ratio across the turbine that this low condensing pressure brings.

Cyclohexane, critical temperature 280.5 °C, is dry and has a decomposition benchmark near 456 °C [51]. It satisfies the five criteria and is placed as a second pure subcritical working fluid, with a condensing pressure of 0.246 bar at 40 °C. It is also a component of the toluene–cyclohexane mixture for which CoolProp carries fitted interaction parameters, and the 50/50 mass mixture is the first mixture case, mixture A. The glide of this mixture

at the evaporation pressures of interest is 4 K, too small for its heating profile to follow the composite.

Table 3. Properties of the working fluids placed on the source (CoolProp).

Fluid	Use in This Study	T_{crit}, °C	p_{crit}, bar	T_{boil}, °C	M, g/mol	p_{cond} at 40 °C, bar	Flammability
Toluene	Pure subcritical; component, mixtures A and B	318.6	41.3	110.6	92.14	0.079	Flammable
Cyclohexane	Pure subcritical; component, mixture A	280.5	40.8	80.7	84.16	0.246	Flammable
n-Pentane	Component, mixture B	196.6	33.7	36.1	72.15	1.16	Flammable
Cyclopentane	Supercritical, 1.25 p_{crit}	238.6	45.8	49.3	70.13	0.74	Flammable
Water	Steam reference	373.9	220.6	100.0	18.02	0.074	None

The second mixture, mixture B, is n-pentane and toluene at 30/70 by mass. Its glide is 24 K at a bubble temperature of 200 °C, and its interaction parameters are fitted as well. The stability of n-pentane is reported to be near 315 °C [13], and the turbine inlet temperature of the mixture is limited to an adopted 300 °C.

Cyclopentane, critical temperature 238.6 °C and critical pressure 45.8 bar, is the supercritical case at 1.25 times its critical pressure, 57.3 bar. Its turbine inlet is held below 300 °C on the basis of the decomposition rates measured by Ginosar et al. [14] (Table 4). At 40 °C, its condensing pressure of 0.74 bar is closer to atmospheric pressure than those of toluene and cyclohexane.

Table 4. Thermal stability, advantages and limitations of the selected working fluids.

Fluid or Mixture	Reported Stability	Main Advantage	Main Limitation	Use in This Study	Maximum Turbine Inlet Temperature (°C)
Toluene	Stable up to about 400 °C [13]	Highest critical temperature of the organic fluids placed; established high-temperature benchmark [7]	0.079 bar condenser at 40 °C; large VFR at this condensing level	Pure subcritical cycle	218.0
Cyclohexane	Decomposition benchmark near 456 °C [51]	0.246 bar condenser at 40 °C; lower VFR than toluene	VFR of 78, above the single-stage threshold	Pure subcritical cycle	236.3
Toluene–cyclohexane 50/50	Constituents: toluene about 400 °C [13]; cyclohexane decomposition benchmark near 456 °C [51]; adopted mixture cap 300 °C	Fitted mixture parameters; both constituents placed as pure fluids	Glide of 4 K at the evaporation pressures of interest	Mixture A	224.9

Table 4. *Cont.*

Fluid or Mixture	Reported Stability	Main Advantage	Main Limitation	Use in This Study	Maximum Turbine Inlet Temperature (°C)
n-Pentane–toluene 30/70	Limited by n-pentane, near 315 °C [13]; adopted mixture cap 300 °C	Glide of 24 K; VFR below 50	Low critical temperature of the pentane component; condensation glide far larger than a 5 K sink rise	Mixture B	243.0
Cyclopentane	270 ppm decomposition after 12 d at 300 °C, about 1500 ppm at 350 °C [14]	Continuous supercritical profile; near atmospheric condenser	57 bar pressure level; large VFR	Supercritical cycle	272.3
Water	Not specified for this comparison	Industry standard; nonflammable	Wet expansion constrained by outlet quality $x_5 \geq 0.88$; isothermal evaporation	Steam reference	—

The set of fluids compared is representative rather than exhaustive. MDM, o-xylene, n-heptane and n-octane were not carried forward. MDM has a critical pressure of 14.2 bar and a working limit near 300 °C [52–54], and its siloxane chemistry lies outside the hydrocarbon set on which the mixtures are built. o-Xylene has stability data from early screening studies [55,56] and a deeper condensing vacuum than toluene. n-Heptane, critical temperature 267 °C, has a reported decomposition threshold near 260 °C [57,58]. n-Octane, critical temperature 296 °C, has been investigated by dilute pyrolysis experiments at 350 to 450 °C [59]. Table 3 lists the properties of the four organic fluids carried forward and of water, and Table 4 the reported stability, advantages and limitations of the working fluids placed on the source. The reported thermal stability limits in Table 4 are approximate and should be interpreted as indicative rather than exact, since they depend on exposure time and test conditions. Table 4 also gives the highest turbine inlet temperature reached by each organic fluid in any retained design or design of the sensitivity analysis; the margins of these temperatures to the stability limits are given in Section 5.6.

Figure 3 shows the saturation domes of the five pure fluids in the temperature–entropy plane against the supply temperatures of the three streams. The critical temperatures of toluene, cyclohexane and cyclopentane lie between the supply temperatures of the bypass gas and the cooler exhaust, whereas that of n-pentane lies below the bypass gas temperature, and the critical temperature of water exceeds all three supply temperatures. However, the operating pressures and temperatures of each cycle are determined by the pinch-constrained cycle optimization of Section 3.6, not by the critical temperatures alone.

3.9. False Air Case

The false air of each of the two preheater strings follows from the rise in oxygen between the calciner cyclone and the string outlet, on dry gas, by the oxygen balance for a nonreacting mixing process, the method used in cement plant audits [32],

$$r = \frac{y_{O_2,out} - y_{O_2,in}}{y_{O_2,air} - y_{O_2,out}} \tag{23}$$

where r is the volume of false air per volume of gas entering the tower, $y_{O2,in}$ and $y_{O2,out}$ the dry oxygen fractions at the cyclone and the outlet, and $y_{O2,air} = 20.95\%$. Because the ratio is taken to the gas entering the tower, the false air volume of a string is r times its dry outlet flow divided by $(1 + r)$. The removable excess is the total false air of the tower less the metered airlift air and the acceptable leakage set by the plant,

$$\dot{V}_{fa} = \sum_j \frac{r_j \dot{V}_{d,j}}{1 + r_j} - \dot{V}_{al} - 0.06 \sum_j \frac{\dot{V}_{d,j}}{1 + r_j} \tag{24}$$

where $\dot{V}_{d,j}$ is the dry outlet flow of string j and $\dot{V}_{al}$ the airlift blower air. With the readings of the plant balance, Equation (24) gives 46,031 Nm^3/h of false air in total, 18,196 Nm^3/h of leakage net of the airlift air and a removable excess of 5983 Nm^3/h. Both the false air ratios and the 6% acceptable leakage are taken on the gas entering the tower, for which Equation (23) defines the ratio, and this removable excess forms the false air case on the consistent basis. The plant's own accounting applies the same percentages (Section 2) to the outlet flows and gives 15,210 Nm^3/h, which is carried as a second false air case on the plant accounting basis.

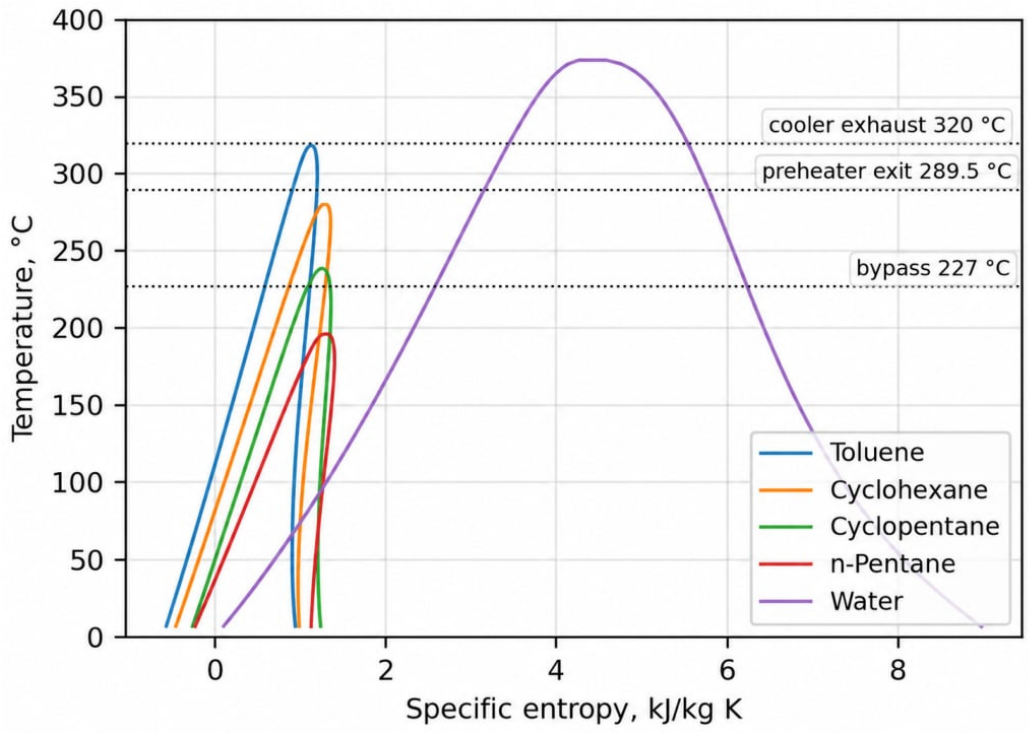

Figure 3. Saturation domes of the five pure fluids with the supply temperatures of the three exhaust streams.

The removable false air enters the preheater at the 33 °C ambient and leaves in the exit gas at 289.5 °C. Removing it changes the preheater exit stream in three ways, all of which follow from one mixing balance: the mass flow falls by the mass of the air removed, the composition changes as the oxygen and nitrogen of that air are taken out, and the temperature rises to the value that the remaining gas would have if the leakage had not cooled it,

$$\left(\dot{m}_g + \dot{m}_{fa}\right)\bar{h}(T_{exit}) = \dot{m}_g\,\bar{h}'(T') + \dot{m}_{fa}\,\bar{h}_{air}(T_{amb}) \tag{25}$$

where $\dot{m}_g$ is the mass flow of the gas without the excess false air, $\dot{m}_{fa}$ the mass flow of the excess false air and T' the corrected exit temperature. The enthalpy above the ambient $\bar{h}$ follows from the heat capacity integral of Equation (3) per unit mass, evaluated for the measured composition on the left and for the corrected composition on the right. Equation (2)

is evaluated at the corrected composition at every temperature, so the enrichment of the remaining gas in CO_2 and H_2O enters both the corrected exit temperature and the corrected composite. Starting from the measured flow and composition, the removal raises the exit temperature from 289.5 to 294.5 °C for the removable excess of 5983 Nm^3/h on the consistent basis, and to 302.5 °C for the plant accounting figure of 15,210 Nm^3/h. The composite curve, the placement of every cycle and the net power target are recomputed with the preheater stream so modified and the other two streams unchanged.

The false air effect is the difference between the net power targets with and without the removable false air. It is evaluated in two forms. The first is at the fixed base-case design, in which the cycle state points of the retained design, set by its operating pressure, its turbine inlet state and, in the organic cycles, its recuperator, are held and the working-fluid mass flow is determined again by Equation (9) for the corrected source. In this design, the effect is a paired difference, computed with both targets under the same perturbations of the measured inputs (Section 3.10). The second is with the cycle reoptimized for the corrected source by repeating the design search of Section 3.6 within the limits in Table 2.

3.10. Sensitivity and Uncertainty

The 5 K source to the working-fluid approach is the optimistic targeting basis of the study, not a practical exchanger design. The placement is also repeated at prescribed approaches of 10 and 20 K for every fluid. These placements show the sensitivity of the targets to a larger approach and do not quantify a fouling layer. Fouling of the gas side surfaces adds heat transfer resistance that lowers the heat recovered by a specified exchanger, and gas-side pressure losses add fan power; both reduce the realizable power below the targets. Their magnitude depends on the exchanger geometry, the gas velocities and the fouling and cleaning conditions of the selected equipment, and neither is modeled. The economically optimal exchanger approach is not determined in this study. The exit limits are varied in three further cases: the mill-on mode, which uses the 202 °C preheater limit of Section 3.3, and the bypass floor and cooler floor cases, in which the limits of the bypass gas and the cooler exhaust are set to 180 and 100 °C, respectively.

The sensitivity analysis examines the entrained dust, the mixture compositions, the supercritical pressure and the component efficiencies at the values in Table 2, one factor at a time in the base case. The dust of the preheater and bypass gases is included in the capacity rates of Section 3.2, and the placement of each cycle is repeated with the search procedure of Section 3.6. Each composition and pressure variant is placed again with the same procedure and constraints, the mass fractions being converted to mole fractions for the property model. For the efficiency variants, the design parameters of the retained designs are held, and the cycle states, the recuperator and the admissible mass flow are recomputed by the placement of Equation (9). These sensitivities are reported separately from the measurement uncertainty treated at the end of this section.

In addition, the steam superheat is searched up to its limit (Section 3.7) in the nine operating and constraint cases of the study: the base case, the two false air cases, the mill-on, the bypass floor and cooler floor cases, the minimum approaches of 10 and 20 K, and the case with the single-stage threshold of VFR $\leq$ 50 imposed. In the last case, the design search of Section 3.6 is repeated with the threshold as a constraint for the cycles whose retained designs exceed it. Equation (21) is satisfied for every design, either by its evaluated condensation path or, for the designs whose paths are not evaluated, by the temperature bound of Section 3.7.

Four further cases are evaluated in the retained designs with the settings in Table 2: the lowest condensing pressure, a working-fluid pressure drop, the mill-off designs operated with the raw mill running and the turbine efficiencies of axial turbines. First, each cycle is

placed at the lowest condensing pressure that meets Equation (21) with the 5 K approach under the base-case cooling water, and mixture B is run in addition with cooling-water temperature rises of 15 and 20 K.

Second, a working-fluid pressure drop, Δp, of 0.1 and 0.2 bar is applied at the retained designs, with the pump delivering $p_{\mathrm{evap}} + \Delta p$ and the turbine inlet state held; the heating curve is rebuilt and Equation (9) is solved again. The drop is placed at two assumed locations, each an isenthalpic pressure reduction. When the drop is placed before the source exchangers, the liquid is throttled to p_{evap} and heated at p_{evap}; when it is placed after them, the fluid is heated at $p_{\mathrm{evap}} + \Delta p$ to the turbine inlet enthalpy and then throttled. Third, the mill-off designs are operated in the mill-on mode with their cycle states held and the mass flow determined again by Equation (9).

Fourth, turbine efficiencies for one-, two- and three-stage axial turbines at optimized speed are taken from the correlation of Macchi and Astolfi [60], Equation (A1), as functions of the size parameter, SP, a turbine size measure defined in Appendix A, and the isentropic volume ratio, V_{r}, of the expansion. As for the efficiency variants, the design parameters of the retained designs are held, and the cycle states, the recuperator and the admissible mass flow are recomputed by the placement of Equation (9) with the estimated efficiency. The correlation is not applied to steam, whose expansion ends in the wet region. The radial turbine model of White and Sayma [46] is fitted for volume ratios up to 10, below those of the retained designs, and is therefore not used for these estimates. The results of the four cases are given in Section 5.6 and Appendix A.

The measurement uncertainties are propagated into the heat and power targets by the law of propagation of uncertainty [61],

$$u_R = \sqrt{\sum_i \left(\frac{\partial R}{\partial x_i} u_{x_i} \right)^2} \tag{26}$$

where R is the target; x_{i} is a measured quantity; and $u_{\mathrm{x,i}} = a_{\mathrm{i}}/\sqrt{3}$, the standard uncertainty for a rectangular distribution of half-width a_{i}. This is a Type B evaluation: the uncertainty is evaluated from adopted bounds of the measurements rather than from the statistical scatter of repeated observations. Twelve measured inputs are perturbed, with bounds adopted for the measurement types of the plant balance. The three duct flows are bounded by ±5% for the Pitot measurements in the preheater and bypass ducts and by ±10% in the dust-laden cooler exhaust duct, and the three duct temperatures are bounded by ±5 °C. The wet density of the preheater gas, from which its moisture follows, is bounded by ±0.0036 kg/Nm^3, each of the four oxygen readings of the false air balance by ±0.2 percentage points and the metered airlift air by ±5%. The twelve half-widths are engineering estimates adopted in this study for these measurement types, as the plant balance report gives no instrument accuracies; the propagated uncertainty therefore depends on these bounds. The partial derivatives are evaluated in this study as central differences of the placement results at $x_{\mathrm{i}} \pm a_{\mathrm{i}}$. The propagation covers the measured plant inputs. The property model, including the binary interaction parameters of the mixtures (Section 4.5), is not part of the propagation, since the fit of these parameters [47] gives no uncertainty bounds.

At the fixed design, $\dot{W}_0$ is the net power target with the measured preheater exit stream and $\dot{W}_1$ the target with the removable false air taken out. The false air effect $D = \dot{W}_1 - \dot{W}_0$ depends on the same measurements as both targets. It is therefore propagated as the difference between the two targets under the same perturbation of each input, a paired difference,

$$u_D = \sqrt{\sum_i \left(\frac{D(x_i + a_i) - D(x_i - a_i)}{2\sqrt{3}} \right)^2} \tag{27}$$

in which both placements are perturbed together by each input over its half-width a_{i}, the removable volume of Equation (24) is recomputed from the same measured inputs in

every perturbation, and the factor $\sqrt{3}$ converts the half-width to the standard uncertainty. Equation (27) retains the dependence that the shared measurements create between $\dot{W}_1$ and $\dot{W}_0$, consistent with the propagation of correlated inputs [61]; the sum of their separate uncertainties would not retain it. Results are reported with the standard uncertainty, which corresponds to a coverage factor of k = 1, and, where an interval is given, with the k = 2 interval $\pm 2u$. The difference between the net power targets of two cycles placed on the same measured streams is propagated as a paired difference using Equation (27).

3.11. Solution Procedure

The calculation runs in five steps. First, the stream table is built from the plant balance by Equations (1)–(3) and checked against it. Second, the composite curve and the cascade of Equations (4)–(7) are built for each set of exit limits, and the source exergy is evaluated by Equation (8). Third, for each cycle and each value of its design variables, the cycle states are computed by Equations (12)–(17) and the fluid heating curve is built at its operating pressure. The placement of Equation (9) is then solved by bisection on the fluid mass flow, with the approach checked at the settings in Table 2. Fourth, the design that maximizes Equation (18) is retained, the stream outlets follow from Equation (10), and Equations (19), (20) and (22) give the exergy destruction and the volume flow ratio. The condensation of the retained design is checked by Equation (21). Fifth, the false air case of Equations (23)–(25) and the sensitivities of Section 3.10 are run, and the uncertainties of Equations (26) and (27) are obtained from the perturbed placements. The sequence is shown in Figure 4. The arrangements of the source exchangers (Section 3.6) are evaluated separately at the retained designs by Equation (11).

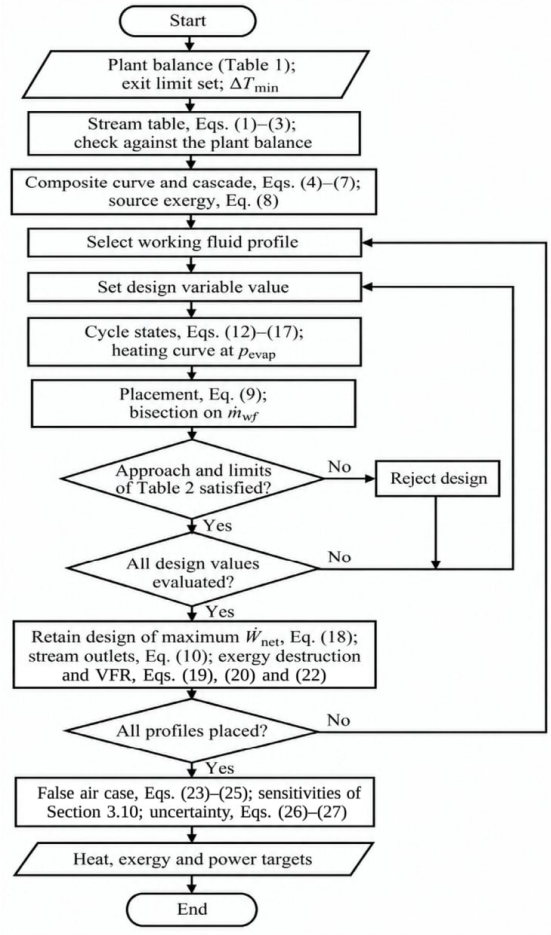

Figure 4. Calculation sequence of the targeting study.

4. Model Validation

Before the model was applied to the exhaust streams of the cement line, the targeting algorithm was verified against the four-stream example of Kemp [18]; the cycle, placement and mixture cycle models were compared with published calculations; and the mixture properties were compared with measured equilibrium data. The comparisons with published calculations and measured data are presented in Figure 5, and all comparisons are summarized in Table 5. The references are Lai et al.'s [6] for the cycle, Hu et al.'s [62] for the placement, Andreasen et al.'s [9] for the mixture cycle, and Myers's [63] and Li et al.'s [64] for the mixture properties.

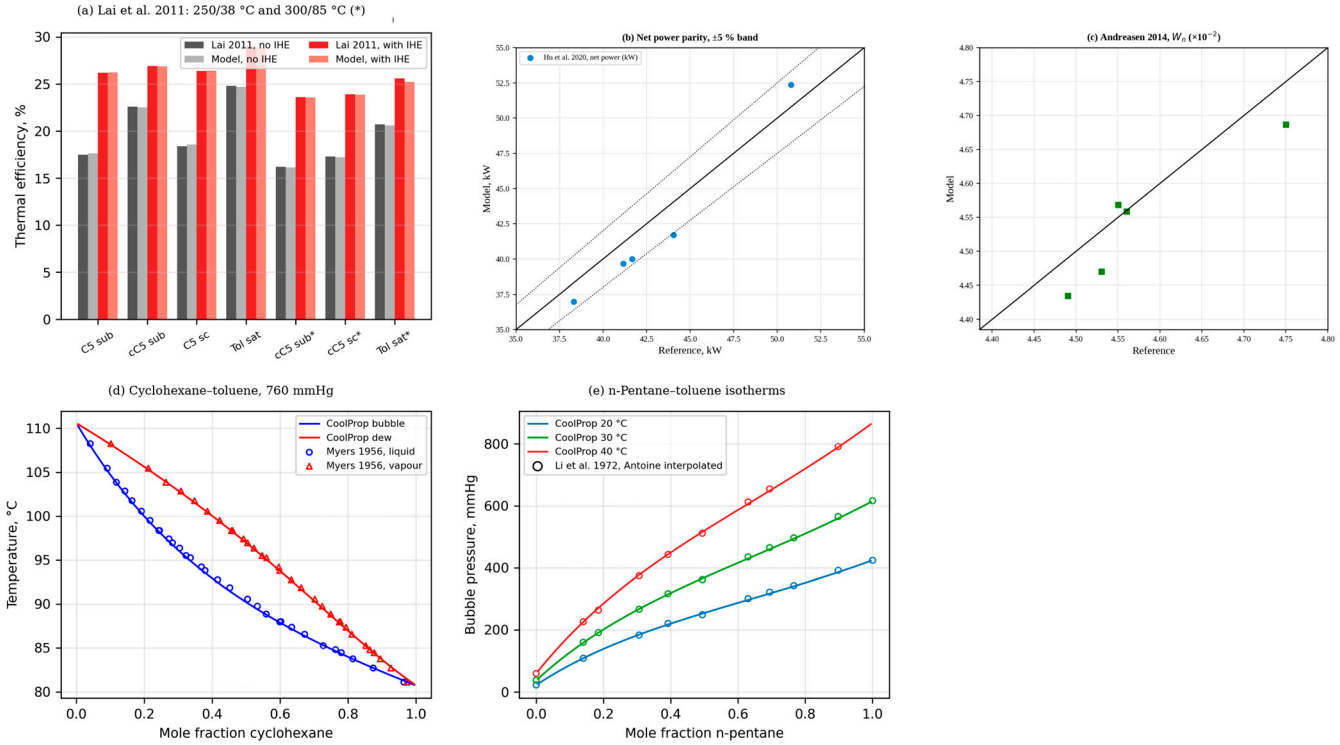

Figure 5. Model validation against published data: (**a**) cycle thermal efficiency [6]; (**b**) net power of optimized designs [62]; (**c**) normalized net power [9]; (**d**) cyclohexane–toluene vapor–liquid equilibrium at 760 mmHg [63]; (**e**) n-pentane–toluene bubble pressure isotherms [64]. In (**a**), asterisks denote maximum and condensation temperatures of 300 and 85 °C, respectively; unmarked cases use 250 and 38 °C. The solid diagonal lines in (**b**,**c**) indicate equality between calculated and reference values; the dotted lines in (**b**) indicate deviations of ±5%.

4.1. Targeting Algorithm

The problem table and cascade of Equations (5)–(7) were run on the four-stream example of Kemp [18] at a minimum approach of 10 K. The model returns a hot utility of 20 kW, a cold utility of 60 kW and a pinch at 85 °C on the shifted temperature scale, the values tabulated by Kemp at the precision he reports. The composite curve of Equation (4) and the shifted cascade form the targeting procedure applied in Section 5 to the three exhaust streams.

Table 5. Validation of the model components against published results.

Component	Reference	Quantity Compared	Cases	Deviation
Targeting algorithm	Kemp [18]	Hot and cold utility, pinch	Four-stream example	None at the reported precision
Cycle model	Lai et al. [6]	Thermal efficiency	7 fluid and condition cases, with and without internal heat exchange	≤0.36 percentage points
Placement	Hu et al. [62]	Net power of optimized designs	5 designs, R1234ze(Z) and R1234ze(E)	−5.3 to +3.1%; 4 of 5 within ±5%
Zeotropic cycle	Andreasen et al. [9]	Normalized net power	5 cases: 4 binary mixtures, superheated propylene	−1.33 to +0.42%
Mixture properties	Myers [63]	Bubble and dew temperature, vapor composition	31 points, cyclohexane–toluene, 760 mmHg	0.21 K mean, 0.45 K max; 0.39 percentage points mean in vapor mole fraction
	Li et al. [64]	Bubble pressure	58 points, n-pentane–toluene, 19.7–41.1 °C	0.87% mean, 2.5% max

4.2. Cycle Model

The cycle model of Equations (12)–(18) was validated against the results of Lai et al. [6], who reported the thermal efficiencies of high-temperature ORC fluids at maximum cycle temperatures of 250 °C with condensation at 38 °C and 300 °C with condensation at 85 °C, with and without an internal heat exchanger. Seven of their cases fall within the fluid set of this study: at a maximum cycle temperature of 250 °C, toluene expanded from saturated vapor, subcritical and supercritical n-pentane and subcritical cyclopentane; at 300 °C, toluene expanded from saturated vapor and subcritical and supercritical cyclopentane. As shown in Figure 5a, the model follows the reference efficiencies case by case, the internal heat exchanger raising the calculated thermal efficiency by 4.2 to 8.6 percentage points across the seven cases. Under their turbine and pump efficiencies and a 10 K cold-end approach in the internal heat exchanger, the model reproduces the fourteen efficiencies of the seven cases, with and without internal heat exchange, within 0.36 percentage points. The largest deviation is for the toluene case with internal heat exchange at a maximum cycle temperature of 300 °C and condensation at 85 °C, with 25.24% calculated against 25.6% reported. The supercritical cyclopentane case, the fluid and cycle type carried into Section 5, agrees within 0.07 percentage points.

4.3. Placement of the Cycle on a Source

The placement of Equation (9) with the cycle model was validated against the optimized designs of Hu et al. [62]. They placed a subcritical ORC on a 120 °C source and reported the net power of the R1234ze(Z) designs selected by four multi-criteria decision-making methods, TOPSIS, LINMAP, VIKOR and WASPAS, and of the maximum power design, which uses R1234ze(E). Their source, sink, pinch and efficiency values were applied, with the condenser pinch taken at the cooling-water outlet as their results imply. As shown in Figure 5b, the calculated net powers range from 37.0 to 52.4 kW. The model

underpredicts the four decision method designs and overpredicts the maximum power design. The deviations are −4.0, −3.6, −3.4 and −5.3% for the TOPSIS, LINMAP, VIKOR and WASPAS designs, respectively, and +3.1% for the maximum power design. Thus, four of the five designs lie within the ±5% band that this study adopts for a reimplementation with a different property library. The WASPAS design lies 0.3 percentage points outside this band, of which up to 0.2 percentage points may come from the precision of its reference power, the reciprocal of a power output ratio given to three digits.

4.4. Zeotropic Mixture Cycle

The mixture treatment of Section 3.7 was validated against the results of Andreasen et al. [9]. They optimized zeotropic mixtures on a 120 °C source and reported the normalized net power, $100\dot{W}_{\mathrm{net}}/(\dot{m}_{\mathrm{hs}}c_{\mathrm{p,hs}}T_{\mathrm{hs,in}})$, the reporting measure of the benchmark, with the inlet temperature $T_{\mathrm{hs,in}}$ taken, as in the benchmark, as its value in °C, 120. This is equivalent to normalizing by the heat the source releases over a 120 K interval, and the quantity is given in Figure 5c as a percentage. Their five benchmark cases are four binary mixtures, isobutane–isopentane, butane–isopentane, butane–pentane and propane–isobutane, and a fifth case of pure superheated propylene. As shown in Figure 5c, the five points lie on both sides of the parity line, on which the calculated and reported values are equal, and the model reproduces the normalized net power within 1.33%, with relative deviations of −0.02, +0.42, −1.31, −1.33 and −1.23%, respectively. The same treatment of evaporation over the glide and of condensation against the rising cooling-water temperature is applied to mixtures A and B in Section 5.

4.5. Mixture Properties

The mixture property predictions were compared with cyclohexane–toluene vapor–liquid equilibrium (VLE) measurements and with n-pentane–toluene bubble pressure measurements. For cyclohexane–toluene at 760 mmHg, the 31 bubble and dew points of Myers [63] are reproduced with a mean absolute deviation of 0.21 K in bubble temperature and a maximum of 0.45 K, and with a mean absolute vapor composition difference of 0.39 percentage points on the mole fraction scale. As shown in Figure 5d, the calculated curves closely follow the measured equilibrium trends over the whole composition range.

For n-pentane–toluene, the 58 bubble pressures of Li et al. [64], measured between 19.69 and 41.12 °C, are reproduced with a mean absolute percentage error of 0.87% and a maximum of 2.5%. Figure 5e shows the 20, 30 and 40 °C isotherms with the measurements interpolated to those temperatures by the Antoine form.

The pressure correction of the liquid-state functions of Section 3.7 was verified separately against the equation of state reference states in the 16 retained mixture designs of the base, false air, mill-on, bypass floor, cooler floor and approach cases (Section 3.10), over the liquid range from the pump outlet to the bubble point. A reference state was accepted when the equation of state, solved directly at the pressure and temperature, returned a liquid whose density lay within 10% of the saturated liquid density at that temperature and whose enthalpy was continuous with the neighboring states. Of the 1327 sampled liquid states, 1280 had accepted references, with maximum differences of 0.051 kJ/kg in enthalpy and 0.13 J/(kg K) in entropy, and the propagation of the accepted references produced no change in heat input, power or minimum approach. The remaining 47 states, for which the direct solution did not return such a liquid, are outside this verification, and no error bound is claimed for them.

The two mixtures are represented by the multi-fluid Helmholtz energy model in CoolProp [37], using composition-dependent reducing functions with the binary interaction parameters of Bell and Lemmon [47], fitted to bubble point measurements that include

the data of Myers [63] and Li et al. [64] compared above. For cyclohexane–toluene, the fit used 504 points from fifteen sources between 20 and 210 °C and 0.03 and 9.1 bar, and for n-pentane–toluene 116 points from two sources between 20 and 111 °C and below 1.2 bar. The condensation temperatures and pressures of both retained designs fall within the overall spans of these data. The evaporation of the retained mixture A design, from 208.5 to 212.3 °C at 12.7 bar, has its bubble point within the temperature span of the cyclohexane–toluene fitting data, its dew point about 2 K above that span and its pressure 3.6 bar above the highest fitted pressure. The evaporation of the retained mixture B design, from 207.3 to 230.7 °C at 18.6 bar, lies about 100 K and 17 bar beyond the n-pentane–toluene fitting data, and these states are predictions of the model beyond its fitting data. Of the toluene–cyclohexane compositions of Section 5.6, 90/10 evaporates within the fitted pressure span and 80/20 to 5/95 lie 0.8 to 7.6 bar above the highest fitted pressure of the cyclohexane–toluene data. The n-pentane–toluene compositions of Section 5.6 lie 10 to 29 bar above the highest fitted pressure of their data. Pure cyclohexane is represented by its own equation of state, with no mixture parameters.

Table 5 summarizes the deviations of each comparison in its own measure. Four of the five placement cases satisfy the adopted ±5% band, and in the other comparisons the model reproduces the published results within the deviations listed in Table 5.

5. Results and Discussion

The results follow the calculation from the source to the cycles. Sections 5.1–5.6 give the targets of the source, the placement of the working fluids, the source-exchanger arrangements, the exergy destroyed in the source exchangers, the effect of the removable false air and the sensitivities, and Sections 5.7 and 5.8 compare the results with published cement studies and draw the implications for the cement line.

5.1. Heat and Exergy Targets of the Source

Figure 6 shows the hot composite curve of the three streams above their exit limits in the base case, with the raw mill stopped and a minimum approach of 5 K, and with the heat counted from the cold end. The streams carry 39.85 MW above the 150 °C cutoffs: 15.8 MW from the preheater exit gas, 9.3 MW from the bypass gas and 14.7 MW from the cooler exhaust. The composite changes slope at the supply temperatures of the streams. Between 320 and 289.5 °C only the cooler exhaust contributes, between 289.5 and 227 °C the cooler exhaust and the preheater gas, and below 227 °C all three. The last interval, 150 to 227 °C, holds 24.5 MW, 62% of the heat, which corresponds to a mean heat capacity flow rate of about 0.319 MW/K, or a slope of 3.14 K/MW in Figure 6. For a specified cycle operating point, each working fluid is placed on this composite by its mass flow: adjusting the mass flow changes the heat absorbed for a given enthalpy rise and therefore the slope and the horizontal extent of the heating profile. A working fluid whose heating curve runs parallel to the composite keeps the approach close to the minimum along the whole interval. A working fluid whose heating curve cannot follow the composite is placed with its limiting point within the interval or at its upper end, and the gap between the two curves widens on one side of that point.

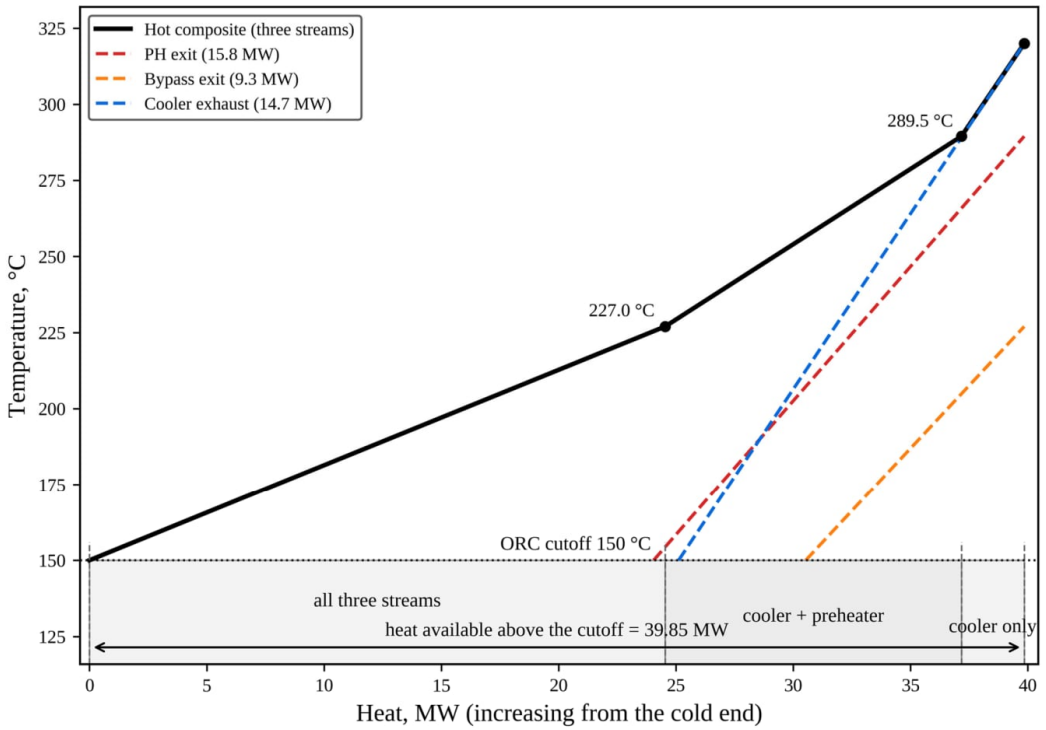

Figure 6. Hot composite curve of the three exhaust streams in the base case, with the individual stream curves.

Figure 7 shows the grand composite curve of the same streams for the base case, for a minimum approach of 20 K and for the mill-on case. The pinch lies at the top of the cascade, at a shifted temperature of 317.5 °C; the hot utility is zero, and the cold utility target is the whole surplus above the cutoffs, 39.85 MW. Raising the approach to 20 K shifts the curve down by 7.5 K without changing the surplus, since every stream still reaches its exit limit. The unchanged surplus does not keep the power targets unchanged: at the larger approach, the organic cycles still absorb the whole surplus, but at lower bubble and turbine inlet temperatures, so their net power targets fall (Section 5.6). In the mill-on case, the 202 °C exit limit of the preheater gas reduces the surplus to 34.06 MW. The fuel oil heating of 428 kW is matched separately by the cooler exhaust between 150 and 145.0 °C and does not enter the cascade.

Table 6 gives the targets for the source and operating cases of the study. The exergy of the surplus in the base case is 15.49 MW, 38.9% of its heat. Raising the exit limit of the bypass gas to 180 °C, in the bypass floor case, removes 3.61 MW of heat and 1.15 MW of exergy, whereas lowering the limit of the cooler exhaust to 100 °C, in the cooler floor case, adds 4.26 MW of heat and 1.06 MW of exergy. Running the raw mill removes 5.79 MW of heat and 1.94 MW of exergy, and removing the excess false air, in the two false air cases, raises the surplus through the higher supply temperature of the preheater exit gas (Section 5.5). In every case, the hot utility is zero. With the entrained dust of the preheater and bypass gases included (Section 3.10), the heat above the cutoffs rises by 0.73 MW, or 1.8%, to 40.58 MW and the source exergy by 0.28 MW to 15.77 MW.

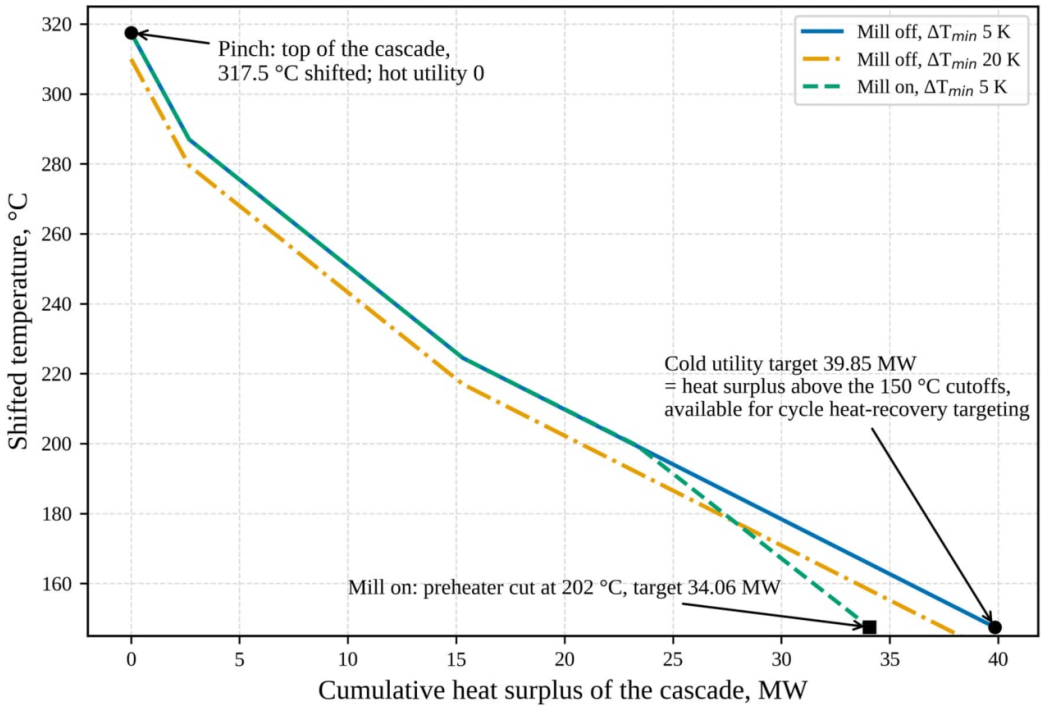

Figure 7. Grand composite curve in shifted temperature for the base case, for a minimum approach of 20 K and for the mill-on case.

Table 6. Heat and exergy targets of the source by case.

Case	Heat Above the Cutoffs (MW)	Cold Utility Target (MW)	Cooler Exhaust, Cutoff → Final (°C)	Fuel Oil Approaches, Hot/Cold End (K)	Source Exergy (MW)
Base, mill off, ΔT_{min} 5 K	39.85	39.85	150 → 145.0	55.3/100.0	15.49
ΔT_{min} 10 K	39.85	39.85	150 → 145.0	55.3/100.0	15.49
ΔT_{min} 20 K	39.85	39.85	150 → 145.0	55.3/100.0	15.49
Mill on	34.06	34.06	150 → 145.0	55.3/100.0	13.55
False air removed, consistent basis	40.10	40.10	150 → 145.0	55.3/100.0	15.64
False air removed, plant accounting	40.50	40.50	150 → 145.0	55.3/100.0	15.87
Bypass floor 180 °C	36.24	36.24	150 → 145.0	55.3/100.0	14.34
Cooler floor 100 °C	44.10	44.10	100 → 95.0	5.3/50.0	16.56
Base, dust included	40.58	40.58	150 → 145.0	55.3/100.0	15.77

5.2. Working-Fluid Placement on the Composite Curve

Figure 8 shows the working-fluid profiles placed against the composite curve in the base case, with the limiting approach of each profile marked by its pair of fluid and source temperatures and the phase regions of the fluid indicated, and Table 7 gives the retained designs. The five organic working fluids, toluene, cyclohexane, mixtures A and B, and supercritical cyclopentane, absorb the whole surplus of 39.85 MW at the minimum approach. Steam absorbs 39.39 MW, so that 0.46 MW of source heat remains unrecovered above the cutoffs. The net power targets are 10.49 MW for supercritical cyclopentane, 10.43 MW for cyclohexane, 10.11 MW for toluene, 10.00 MW for mixture A, 9.25 MW for steam and

8.28 MW for mixture B, and the thermal efficiencies range from 20.8% for mixture B to 26.3% for supercritical cyclopentane (Table 7). At the retained cycle designs, the standard uncertainties of these targets arising from the adopted measurement bounds of Section 3.10 are 0.28 to 0.38 MW. The nominal power differences between the leading fluids are 0.06 MW between supercritical cyclopentane and cyclohexane, 0.32 MW between cyclohexane and toluene, and 0.11 MW between toluene and mixture A. Section 5.6 gives the estimated reductions in turbine efficiency, 0.5 to 2.6 percentage points, at which these power differences vanish, and Section 5.8 compares the differences between the three highest targets with their paired uncertainties.

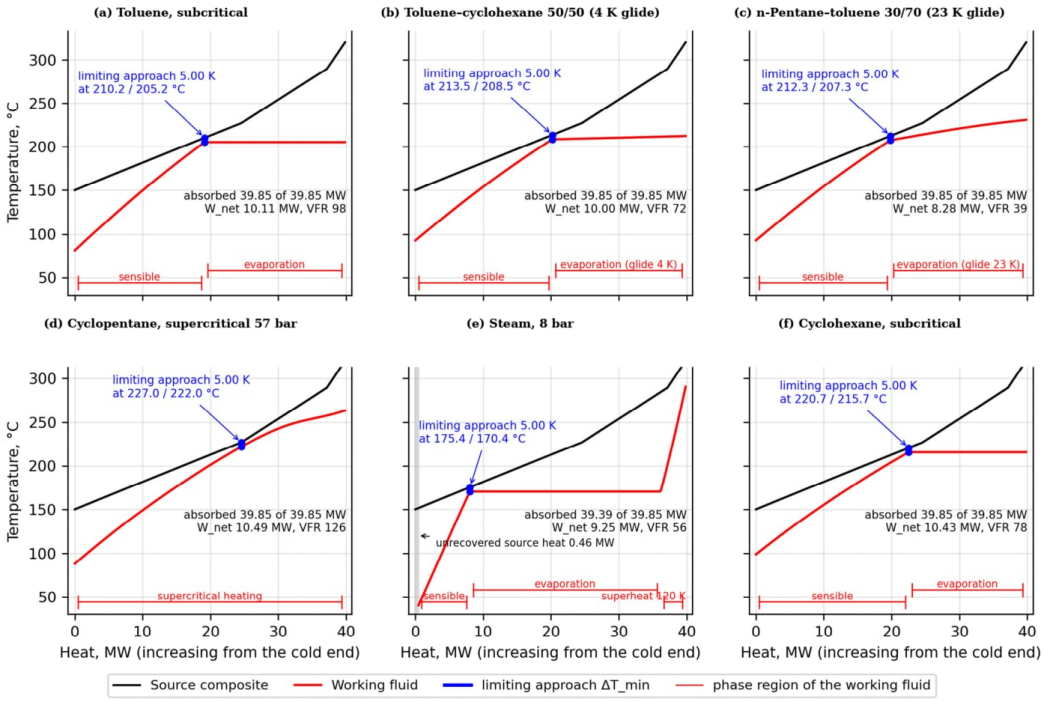

Figure 8. Placement of the working-fluid profiles on the hot composite curve in the base case: (**a**) toluene; (**b**) toluene–cyclohexane 50/50; (**c**) n-pentane–toluene 30/70; (**d**) supercritical cyclopentane; (**e**) steam; (**f**) cyclohexane.

Table 7. Retained designs of the working fluids in the base case, with the raw mill off and a minimum approach of 5 K.

Cycle	Design	p_{evap} or p (bar)	$\dot{W}_{net}$ (MW)	η_{th} (%)	VFR	Limiting Approach, Fluid/Gas (°C)	$\dot{E}_D$ (MW)	$u(\dot{W}_{net})$ (MW)
Toluene, subcritical	T_{bubble} 205.19 °C	8.2	10.11	25.4	98	205.2/210.2	2.28	0.34
Cyclohexane, subcritical	T_{bubble} 215.74 °C	17.1	10.43	26.2	78	215.7/220.7	1.80	0.38
Toluene–cyclohexane 50/50 (A)	T_{bubble} 208.48 °C, glide 3.8 K	12.7	10.00	25.1	72	208.5/213.5	1.98	0.35
n-Pentane–toluene 30/70 (B)	T_{bubble} 207.33 °C, glide 23.4 K	18.6	8.28	20.8	39	207.3/212.3	1.72	0.28
Cyclopentane, supercritical	T_4 263.68 °C, 1.25 p_{crit}	57.3	10.49	26.3	126	222.0/227.0	1.49	0.37
Steam	8 bar, 120 K superheat	8.0	9.25	23.5	56	170.4/175.4	3.10	0.29
Steam, extended search	8 bar, 144.6 K superheat	8.0	9.32	23.8	54	170.4/175.4	2.98	—

In every base-case placement of Figure 8, the temperature difference between the composite curve and the working fluid falls to the minimum approach of 5.00 K, but the point at which this occurs differs between the fluids and follows from the shape of each heating curve against the composite. For the pure fluids in subcritical cycles, toluene, cyclohexane and steam, the temperature difference decreases along the liquid preheating and reaches its minimum at the bubble point. Beyond this point, moving from left to

right in Figure 8, the source temperature continues to rise while the fluid evaporates at constant temperature, so the gap between the two curves widens. For toluene (Figure 8a), the minimum approach is therefore reached at 205.2 °C on the fluid side against 210.2 °C on the composite, where the evaporation plateau comes closest to the sloping source curve. For cyclohexane (Figure 8f), it is reached at 215.7 °C against 220.7 °C. Cyclohexane thus evaporates 10.5 K above toluene. Its net power target is 3% higher (Table 7). The two mixtures, in contrast, evaporate over a temperature glide. Mixture A, toluene–cyclohexane 50/50 by mass, evaporates almost isothermally: its glide of 3.8 K is too small for its heating profile to follow the composite. Its bubble point of 208.5 °C lies 3.3 K above that of toluene, while its net power is 1% lower. Mixture B, n-pentane–toluene 30/70 by mass, evaporates over a glide of 23.4 K, and its heating profile follows the composite from its bubble point at 207.3 °C. However, the design retained at maximum power for this mixture has the lowest thermal efficiency of the six working fluids, 20.8%. Since it absorbs the same 39.85 MW as the other organic cycles, it has the lowest net power target among them. Its target is also below that of steam, which absorbs 0.46 MW less heat but at a thermal efficiency of 23.5%.

Supercritical cyclopentane, at 57.3 bar, is heated without a phase change, so its continuous heating curve has no evaporation plateau. In the placement, its mass flow is adjusted until the minimum temperature difference from the composite reaches 5 K, and the calculated minimum lies at 227 °C on the composite, the breakpoint where the bypass gas begins to contribute, with the fluid at 222.0 °C. Among the six base designs, it is the only one whose minimum approach lies at a breakpoint of the source rather than at the start of evaporation of the fluid. Section 5.6 shows how each of these limiting locations shapes the design sweeps.

Steam at 8 bar (Figure 8e) evaporates at 170.4 °C against 175.4 °C on the composite. The retained steam reference, at 8 bar and the adopted upper superheat bound of 120 K, gives a turbine outlet quality of 0.912, above the minimum of 0.88. At the superheat limit set by the source (Section 3.7), 144.6 K at 8 bar, the steam target rises to 9.32 MW and the turbine outlet quality to 0.925; this design is listed in Table 7 as a second steam design. In this design, the prescribed 5 K approach is also active at the hot end of the source, and lowering the cooler exhaust temperature by 5 °C, one of the perturbations of the uncertainty procedure of Section 3.10, leaves no feasible turbine inlet state in the fixed design. The uncertainty propagation and the paired false air comparison therefore use the 120 K design as the steam reference, and the design of the extended search is reported beside it. The net power target of supercritical cyclopentane exceeds those of the extended search design and the reference by 1.17 and 1.24 MW, respectively.

The cycles differ in their volume flow ratios as well as in their power (Table 7). With a VFR of 39, the mixture B design is the only one of the six base designs below the single-stage screening threshold of 50 [8], and steam, at 56, is just above it. Toluene at 98, cyclohexane at 78, mixture A at 72 and supercritical cyclopentane at 126 exceed the threshold at the common 40 °C condenser outlet and are therefore flagged for further expander assessment, including multistage expansion (Section 3.7). These ratios follow from the turbine inlet and outlet states: toluene, cyclohexane and mixture A condense at 0.08 to 0.25 bar, and supercritical cyclopentane enters the turbine at 57.3 bar. The operating pressures of the organic cycles range from 8.2 bar for toluene to 57.3 bar for supercritical cyclopentane, and the working-fluid mass flows of the five organic cycles lie between 71.7 and 75.2 kg/s, against 13.7 kg/s for steam.

The condensing conditions of the retained designs are given in Table 8, with the approach verified along the condensation path by Equation (21). Under the common 40 °C saturated liquid outlet and cooling-water conditions, the pure organic fluids reach their minimum approach, 5.08 to 5.14 K, at the start of condensation, where desuperheating

ends, and steam its minimum approach of 5.00 K at the wet turbine exit. Mixtures A and B condense over glides of 7.7 and 38.4 K, respectively, and reach their minimum, 10 K, at the cold end, where the 40 °C liquid outlet faces the cooling water entering at 30 °C (Table 8). The condensing pressures and the condensation profiles differ between the fluids, and every design satisfies the prescribed 5 K approach throughout condensation. For the 52 designs of the sensitivity analysis, the minimum lies between 5.00 and 5.15 K for the 24 pure fluid and steam designs and between 5.79 and 10.00 K for the 28 mixture designs. For the toluene–cyclohexane compositions, the minimum moves from the cold end through interior points of the path to the start of condensation as the composition approaches pure cyclohexane and the glide vanishes.

Table 8. Condensation of the retained base designs against the cooling water.

Cycle	Condenser Inlet (°C)	p_{cond} (bar)	Glide (K)	Temperature Difference, Hot/Cold End (K)	Minimum Approach (K)	Location of the Minimum
Toluene, subcritical	45.5	0.079	0	10.5/10.0	5.08	Start of condensation
Cyclohexane, subcritical	46.1	0.246	0	11.1/10.0	5.11	Start of condensation
Toluene–cyclohexane 50/50 (A)	48.7	0.182	7.7	13.7/10.0	10.00	Cold end, liquid outlet
n-Pentane–toluene 30/70 (B)	79.4	0.553	38.4	44.4/10.0	10.00	Cold end, liquid outlet
Cyclopentane, supercritical	49.0	0.740	0	14.0/10.0	5.14	Start of condensation
Steam	40.0	0.074	0	5.0/10.0	5.00	Hot end, turbine exit

5.3. Source-Exchanger Arrangements and Recovery Targets

The composite target is obtained on the assumption that the hotter streams can serve more than one section of the working-fluid heating curve, as vertical matching between the composite curve and the heating curve requires. Table 9 reports what the series arrangement, the simplest of the three, achieves: the working fluid passes through the three source exchangers in series, taking heat first from the bypass gas, then from the preheater gas and last from the cooler exhaust, each stream cooled no lower than its exit limit. For toluene, the bypass gas heats the fluid from 81.4 to 145.3 °C and delivers 9.31 MW. The preheater gas then heats it to its evaporation temperature, 205.2 °C, and evaporates part of it, delivering 15.77 MW. The cooler exhaust therefore meets a fluid at 205.2 °C and can be cooled only to 210.2 °C at the minimum approach, so it delivers 9.57 MW of its 14.7 MW and leaves 5.2 MW of its heat above the cutoff unrecovered. As a result, toluene absorbs 34.65 MW in the series arrangement, 87.0% of the composite heat target, and does not reach the retained turbine inlet state.

For the other cycles, the heat absorbed in the series arrangement at the retained mass flow is 82.9 to 88.5% of the heat target (Table 9), and at this mass flow none of them reaches the retained inlet state. These fractions are fractions of absorbed heat, not of net power. The operating point basis gives the power: with the cycle states and efficiencies of the retained designs held, the fluid reaches the turbine inlet state in the series arrangement at 72.4 to 88.5% of the retained mass flow, and the net power falls to 6.48 to 8.46 MW (Table 10). Toluene then gives the most power, whereas supercritical cyclopentane loses most, 27.6% of its net power target, because at this reduced flow the cooler exhaust, last in

the series, meets the continuously heated cyclopentane at 247.7 °C. This shortfall illustrates why the composite targets in Table 7 are thermodynamic upper bounds on the recovery that a heat exchanger network realizes with each evaluated cycle at its specified operating conditions, the adopted efficiencies and the exit limits of Section 3.3 [18,25]. The idealized two-section split-flow arrangement, in contrast, approaches them under the adopted heat transfer constraints (Table 10).

Table 9. Heat absorbed in the series and parallel preheating arrangements as a fraction of the composite heat target.

Cycle	Heat Absorbed at the Composite Target (MW)	Series Arrangement		Parallel Preheating Arrangement		Retained Inlet State Reached
		Heat Absorbed (MW)	Fraction of the Heat Target	Heat Absorbed (MW)	Fraction of the Heat Target	
Toluene, subcritical	39.85	34.65	87.0%	33.00	82.8%	no
Cyclohexane, subcritical	39.85	33.06	83.0%	31.81	79.8%	no
Toluene–cyclohexane 50/50 (A)	39.85	33.79	84.8%	32.55	81.7%	no
n-Pentane–toluene 30/70 (B)	39.85	33.35	83.7%	32.12	80.6%	no
Cyclopentane, supercritical	39.85	33.02	82.9%	31.41	78.8%	no
Steam	39.39	34.86	88.5%	36.62	93.0%	no

Table 10. Operating points at the composite target and in the series and split-flow arrangements.

Cycle	Arrangement	$\dot{m}_{wf}$ (% of Target)	$\dot{W}_{net}$ (MW)	$\dot{E}_D$ (MW)	η_{II} (%)	η_{conv} (%)
Toluene, subcritical	Composite target	100.00	10.11	2.28	65.2	76.5
	Series	83.77	8.46	2.26	63.5	76.5
	Two-section split flow	99.99	10.10	2.28	65.2	76.5
Cyclohexane, subcritical	Composite target	100.00	10.43	1.80	67.3	76.2
	Series	79.46	8.29	1.84	65.1	76.2
	Two-section split flow	99.96	10.42	1.80	67.3	76.2
Toluene–cyclohexane 50/50 (A)	Composite target	100.00	10.00	1.98	64.5	74.0
	Series	81.25	8.12	2.00	62.6	74.0
	Two-section split flow	100.00	10.00	1.98	64.5	74.0
n-Pentane–toluene 30/70 (B)	Composite target	100.00	8.28	1.72	53.5	60.2
	Series	78.26	6.48	1.76	51.7	60.2
	Two-section split flow	99.99	8.28	1.72	53.5	60.2
Cyclopentane, supercritical	Composite target	100.00	10.49	1.49	67.7	74.9
	Series	72.35	7.59	1.42	65.7	74.9
	Two-section split flow	99.83	10.47	1.49	67.7	74.9
Steam	Composite target	100.00	9.25	3.10	60.3	75.5
	Series	88.51	8.19	3.07	58.8	75.5
	Two-section split flow	100.00	9.25	3.10	60.3	75.5

In the parallel preheating arrangement at the retained mass flow, the organic working fluids absorb 78.8 to 82.8% of their 39.85 MW heat target and steam 93.0% of its 39.39 MW, and none of them reaches the retained turbine inlet state (Table 9), because the whole remaining heating duty then falls on the preheater gas alone. In the split-flow arrangement of Section 3.6 (Figure 9), the boundary between the sections found by the search lies in the evaporation of the subcritical fluids and at a fluid temperature of 222.0 °C for supercritical cyclopentane (Table A1). For the organic fluids, the preheater gas and the cooler exhaust pass from their upper to their lower exchangers near 227 °C, the supply temperature of the bypass gas and a breakpoint of the composite. With this arrangement, the fluid reaches the retained turbine inlet state at 99.8 to 100% of the target mass flow, the net power comes within 0.2% of the targets, and the nominal ranking of the fluids is unchanged (Table 10). Pinch network design uses stream splitting of this kind to reach the targets [18]. Table A1 gives the allocation found by the search, a feasible allocation of heat rather than a sized network.

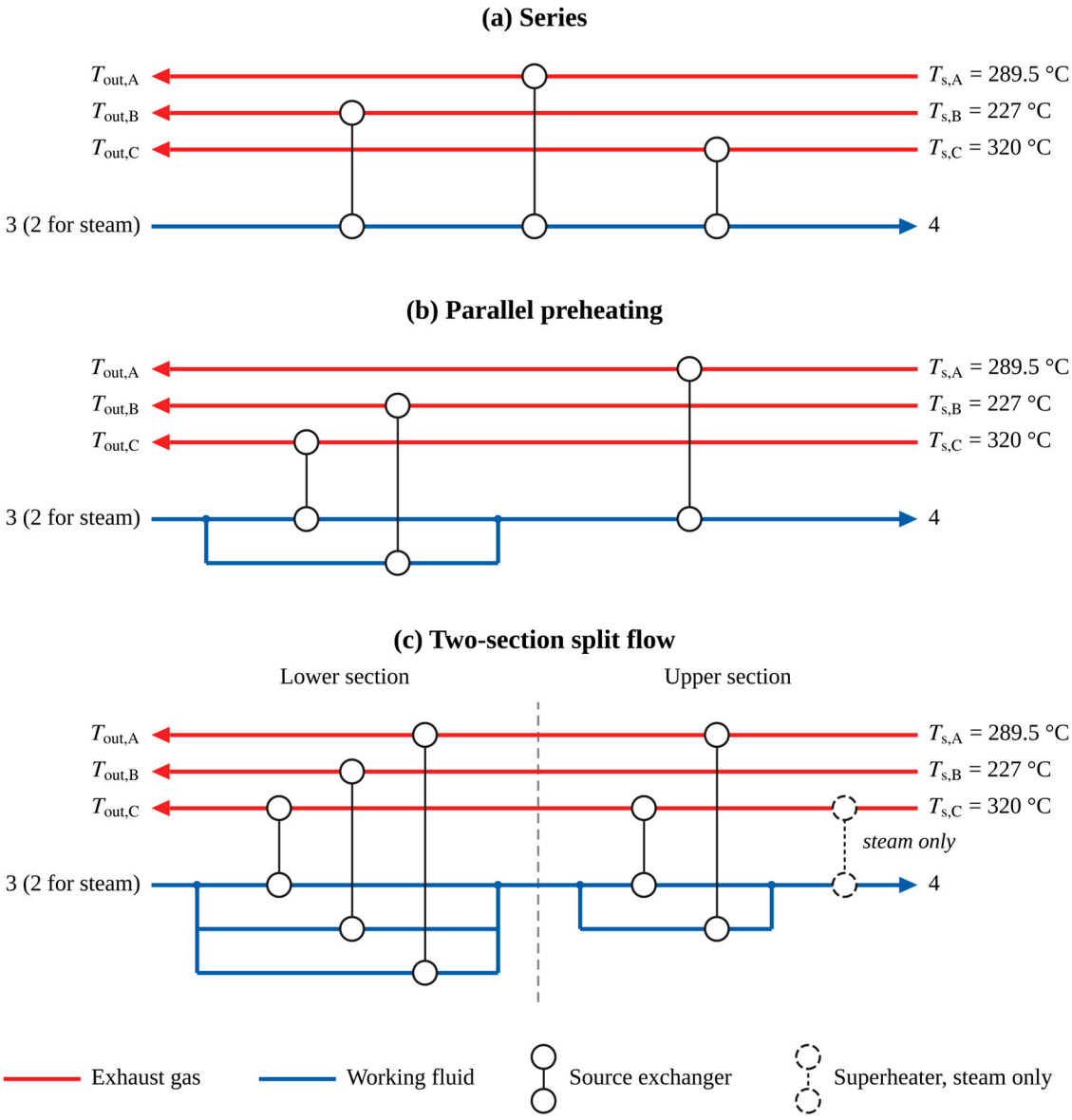

Figure 9. Grid diagrams of the three source-exchanger arrangements: (**a**) series; (**b**) parallel preheating; (**c**) idealized two-section split flow.

5.4. Exergy Destroyed in the Source Exchangers

Figure 10 shows the net power target and the exergy destroyed in the source exchangers for the working fluids in the base case and in the false air, mill-on, bypass floor and cooler floor cases, and Table 11 gives the values. As shown in Figure 10a, the false air and cooler floor cases raise all six targets and the mill-on and bypass floor cases lower them, while the nominal ranking of the fluids stays the same in every case. Figure 10b shows that the fluids rank differently by exergy destruction than by net power. In the base case, the destruction rises from 1.49 MW for supercritical cyclopentane through mixture B, cyclohexane, mixture A and toluene to 3.10 MW for steam, 9.6 to 20.0% of the 15.49 MW of source exergy. Mixture A destroys less source-exchanger exergy than toluene but also produces slightly less power. Cyclohexane, whose plateau at 215.7 °C lies above the 205.2 °C plateau of toluene and the 208.5 °C bubble point of mixture A, destroys less than both and produces more power than either. The continuous heating curve of supercritical cyclopentane follows the composite most closely, so its source exchangers destroy the least exergy. In contrast, the evaporation plateau of toluene and the almost isothermal evaporation of mixture A open a widening gap between the composite and the fluid curve above the bubble point, and the isothermal evaporation of steam at 170.4 °C opens the widest gap.

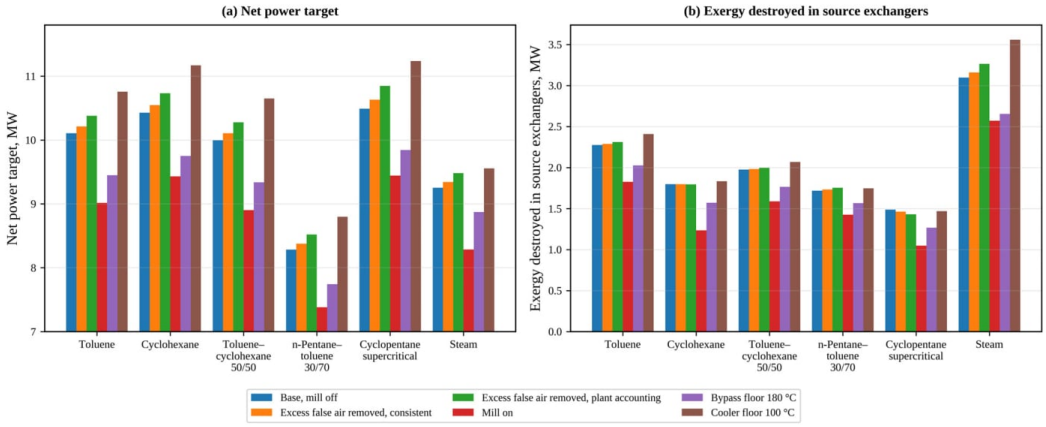

Figure 10. Net power target (**a**) and exergy destroyed in the source exchangers (**b**) of the working fluids by case.

Table 11. Net power target and, in parentheses, exergy destroyed in the source exchangers (MW) of the working fluids by case, each from its own design search.

Cycle	Base	Base, Dust Included	False Air, Consistent Basis	False Air, Plant Accounting	Mill On	Bypass Floor 180 °C	Cooler Floor 100 °C	ΔT_{min} 10 K	ΔT_{min} 20 K	VFR ≤ 50
Toluene, subcritical	10.11 (2.28)	10.29 (2.31)	10.21 (2.29)	10.38 (2.31)	9.02 (1.83)	9.45 (2.03)	10.76 (2.41)	9.84 (2.57)	9.28 (3.20)	8.77 (3.77)
Cyclohexane, subcritical	10.43 (1.80)	10.62 (1.83)	10.55 (1.80)	10.73 (1.80)	9.43 (1.24)	9.75 (1.57)	11.17 (1.83)	10.16 (2.11)	9.59 (2.77)	9.61 (2.75)
Toluene–cyclohexane 50/50 (A)	10.00 (1.98)	10.18 (2.01)	10.11 (1.98)	10.28 (2.00)	8.90 (1.59)	9.34 (1.77)	10.65 (2.07)	9.73 (2.28)	9.17 (2.92)	9.29 (2.78)
n-Pentane–toluene 30/70 (B)	8.28 (1.72)	8.44 (1.75)	8.38 (1.73)	8.52 (1.75)	7.38 (1.42)	7.74 (1.57)	8.80 (1.75)	8.05 (1.99)	7.56 (2.56)	8.28 (1.72)
Cyclopentane, supercritical	10.49 (1.49)	10.68 (1.51)	10.63 (1.46)	10.85 (1.43)	9.44 (1.05)	9.84 (1.27)	11.24 (1.47)	10.23 (1.78)	9.68 (2.37)	none
Steam	9.25 (3.10)	9.42 (3.15)	9.34 (3.16)	9.48 (3.27)	8.29 (2.57)	8.87 (2.65)	9.56 (3.56)	8.97 (3.36)	8.44 (4.04)	9.12 (3.36)
Steam, extended search	9.32 (2.98)	—	9.41 (3.04)	9.55 (3.15)	8.32 (2.51)	8.91 (2.59)	9.68 (3.38)	9.04 (3.24)	8.53 (3.90)	9.26 (3.21)

The two measures, source-exchanger exergy destruction and net power, answer different questions. Source-exchanger exergy destruction quantifies the irreversibility of the heat addition and depends on the transferred heat and on the local absolute temperatures of the gas and the working fluid. Net power depends, in addition, on the expansion and pumping and on the internal heat recovery and heat rejection processes. Therefore, a lower exergy destruction in the source exchangers does not necessarily lead to a higher net power. Mixture B shows the difference: it produces the least power despite the second lowest destruction in the source exchangers. Its glide of 23.4 K matches the composite well, and the fluid takes up 13.77 MW of exergy from the source, more than toluene or mixture A. However, the mixture B cycle converts only 60.2% of that exergy into net power, compared with 74.0 to 76.5% for the other five fluids. The mixture also condenses over a temperature glide, and its condensation glide of 38.4 K substantially exceeds the 5 K rise of the cooling water (Table 8), a mismatch consistent with the mechanisms discussed in zeotropic ORC studies [10,11]. The present comparison does not isolate the contribution of this mismatch to the power difference.

Reducing this mismatch by increasing the cooling-water temperature rise to 15 or 20 K does not raise the net power of mixture B above that of its design at the lowest condensing pressure with water heated from 30 to 35 °C, because its minimum condenser approach lies at the cold end, where the water enters at 30 °C (Section 5.6). The distinction between source-exchanger exergy destruction and net power also appears in the arrangements of Section 5.3. For the series arrangement at reduced flow, the second law efficiency, η_{II}, lies 1.4 to 2.2 percentage points below its value at the target, while the conversion efficiency, η_{conv}, is unchanged, since the cycle states are those of the retained designs; the difference arises in the source exchangers, which destroy a larger fraction of the smaller exergy that the gases give up at the reduced flow. The two-section split-flow arrangement keeps η_{conv} at its target value and η_{II} within 0.03 percentage points of its target value (Table 10). The source-exchanger exergy destruction and the net power are therefore read together: the first measures the temperature match in the source exchangers, and the second the performance of the whole cycle.

The ranking of the fluids by exergy destruction is the same in the dust, false air, floor and approach cases; only in the mill-on case does cyclohexane, at 1.24 MW, destroy less than mixture B, at 1.42 MW. Removing the excess false air lowers the destruction of supercritical cyclopentane by 0.02 to 0.06 MW and that of cyclohexane by less than 0.01 MW on the two bases, and raises that of the other cycles by 0.01 to 0.17 MW, most for steam. The hotter preheater gas widens the gap above an evaporation plateau, which raises the destruction, whereas the reoptimized bubble temperatures of the subcritical organic cycles rise and narrow it, most for cyclohexane, by 1.6 K on the consistent basis and 4.1 K on the plant accounting basis. Running the raw mill lowers the destruction of every cycle by 0.29 to 0.56 MW with the heat it removes. In the cooler floor case, lowering the cooler exhaust limit to 100 °C adds heat at the bottom of the composite, where the heating profiles of steam and toluene match it most poorly. This raises the destruction of steam by 0.46 MW and that of toluene by 0.13 MW, against 0.03 to 0.09 MW for cyclohexane and the two mixtures, while that of supercritical cyclopentane changes by 0.02 MW.

5.5. Effect of the Removable False Air

Figure 11 shows the preheater exit stream as measured, its false air amounting to 22.6% of the gas entering the tower, and with the removable false air taken out by the mixing balance of Equation (25): 5983 Nm^3/h on the consistent basis and 15,210 Nm^3/h on the plant accounting basis. The removal raises the exit temperature from 289.5 to 294.5 °C on the consistent basis and to 302.5 °C on the plant accounting basis, and it reduces the mass

flow by 2.15 and 5.46 kg/s, respectively. The heat available above the cutoff rises by 0.26 and 0.65 MW, respectively. Each rise approximately equals the sensible heat that warmed the removed air from the 33 °C ambient to the 150 °C cutoff: this heat lies below the cutoff in the measured stream, and the mixing balance keeps it in the remaining gas, above the cutoff.

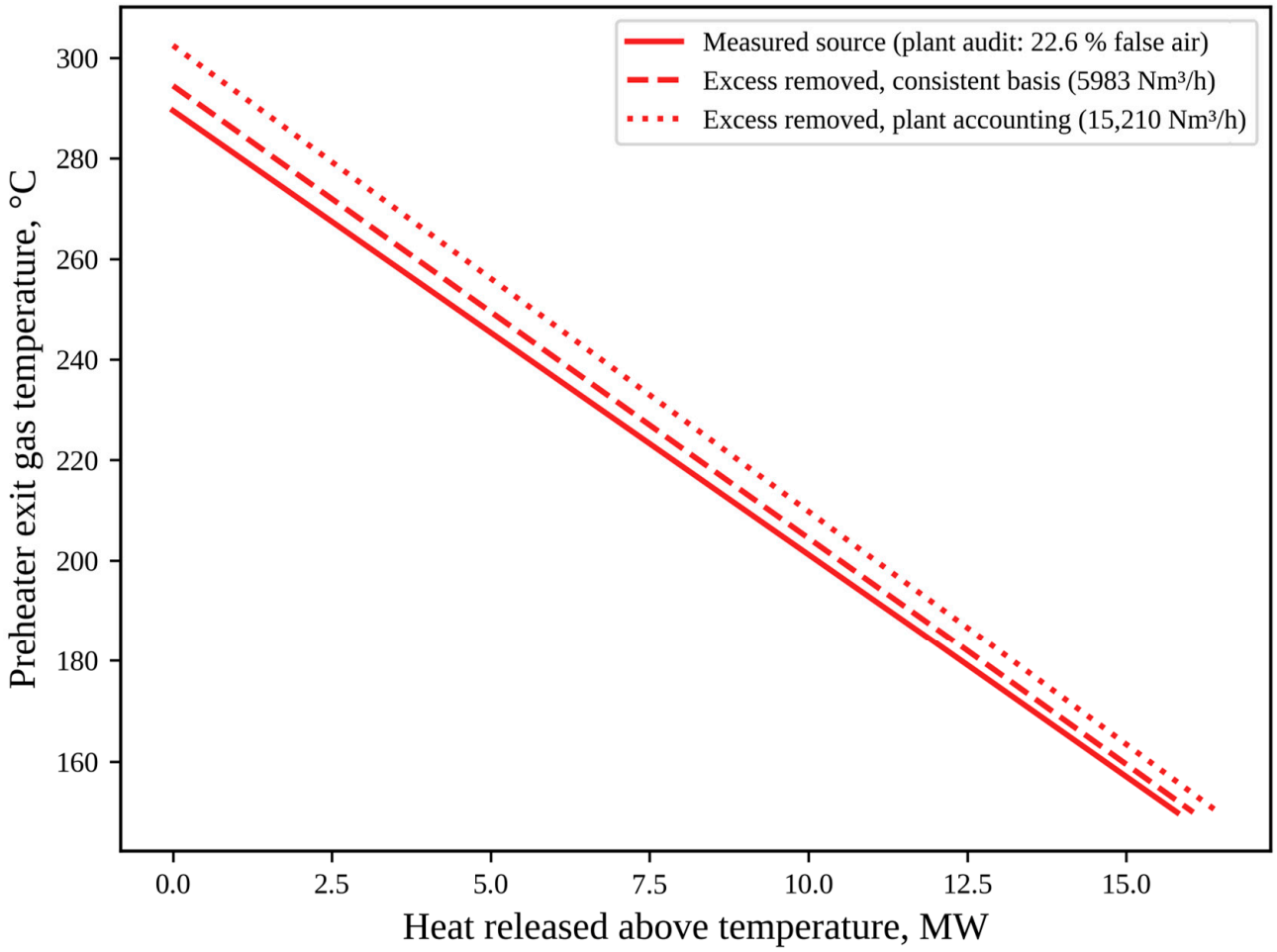

Figure 11. Heat released above a given temperature by the preheater exit gas, as measured and with the removable false air taken out on the consistent and plant accounting bases.

Table 12 gives the false air effect on the net power targets in the two forms of Section 3.9. In the fixed base-case design, with the retained cycle states held and the mass flow determined again for the corrected source, the difference between the targets with and without the removable false air on the consistent basis, the paired difference of Section 3.10, is +0.053 to +0.091 MW, or 0.6 to 1.0% of the base target, with standard uncertainties of 0.028 to 0.105 MW from the adopted measurement bounds. The k = 2 intervals cross zero for the five organic cycles but not for steam. The fixed design of the 120 K steam reference is limited by the minimum approach alone and leaves source heat unrecovered (Section 5.2), whereas the organic cycles in their fixed designs absorb the whole surplus. The paired gain of steam, 0.091 MW, the largest of the six, changes negligibly under the tested perturbations of the duct temperatures and of the bypass and cooler flows, and its standard uncertainty, 0.028 MW, is small against that gain, so its interval remains positive.

Table 12. Effect of removing the excess false air on the net power target: fixed design effect and nominal gains after reoptimization.

Cycle	Fixed Design Effect, Consistent Basis (MW)	u (MW)	k = 2 Interval (MW)	Reoptimized, Consistent Basis (MW)	Reoptimized, Plant Accounting (MW)
Toluene, subcritical	+0.065	0.070	−0.075 to +0.205	+0.107	+0.274
Cyclohexane, subcritical	+0.067	0.100	−0.133 to +0.267	+0.118	+0.303
Toluene–cyclohexane 50/50 (A)	+0.064	0.077	−0.089 to +0.217	+0.109	+0.280
n-Pentane–toluene 30/70 (B)	+0.053	0.061	−0.069 to +0.176	+0.091	+0.235
Cyclopentane, supercritical	+0.067	0.105	−0.143 to +0.277	+0.141	+0.356
Steam	+0.091	0.028	+0.034 to +0.147	+0.091	+0.230

With the cycle reoptimized for the corrected source, the net power gain on the consistent basis is +0.091 to +0.141 MW, 1.0 to 1.3% of the base target, and on the plant accounting basis +0.230 to +0.356 MW, 2.5 to 3.4%. These reoptimized gains are differences between the results of two separate design searches and are nominal values. The uncertainty intervals in Table 12 are therefore those of the fixed design gains, obtained by applying the same measurement perturbations to the source with and without the removable false air in the same cycle design. After reoptimization, supercritical cyclopentane has the largest gain; its retained design, like those of the other organic cycles, moves to a different matched operating point on the revised source curve.

The removable false air on the consistent basis, 5983 Nm^3/h, carries about 0.57 MW of sensible enthalpy above the 33 °C ambient at the measured exit temperature. This heat is supplied by the kiln fuel, and the cement literature accounts for it in terms of fuel and fan power [32]. In the false air case on the consistent basis (Section 3.9), removing the excess false air raises the heat available above the cutoff by 0.26 MW and the reoptimized net power targets by a nominal 0.09 to 0.14 MW. These increases in the recovery potential depend on the removal assumed in the mixing balance of Equation (25), in which the heat that warmed the removed air stays in the remaining gas rather than being saved as kiln fuel. The power gains are differences between two targets, not a conversion of the 0.57 MW of air heating into power. Therefore, false air reduction remains primarily a fuel-saving measure, and its modeled effect on the recovery target is a small increase.

5.6. Sensitivity Analysis

Figure 12 shows the net power targets of the working fluids at prescribed minimum approaches of 5, 10 and 20 K in the source exchangers. Raising the approach from 5 to 10 K reduces the targets by 2.5 to 3.0%, and raising it from 5 to 20 K reduces them by 7.7 to 8.8%; in both cases, supercritical cyclopentane loses the smallest fraction of its target and steam the largest. The nominal ranking of the fluids is unchanged at the tested approaches. The exergy destroyed in the source exchangers rises with the approach for every cycle, from 1.49 to 2.37 MW for supercritical cyclopentane and from 3.10 to 4.04 MW for steam as the approach rises from 5 to 20 K (Table 11).

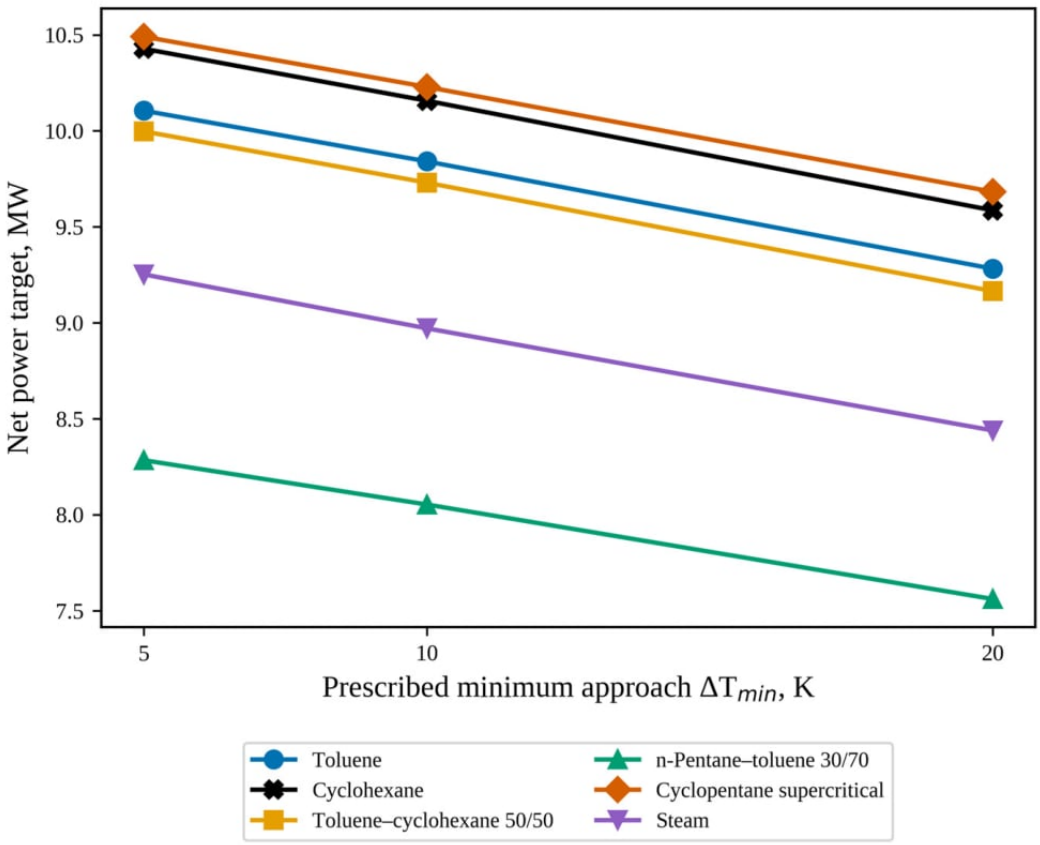

Figure 12. Net power target of the working fluids at prescribed minimum approaches of 5, 10 and 20 K in the source exchangers.

Running the raw mill, which raises the exit limit of the preheater gas to 202 °C, removes 14.5% of the heat above the cutoffs (Table 6) but reduces the net power targets by only 9.6 to 10.9% (Table 11), because the heat removed is the coldest part of the preheater gas. In the bypass floor case, with the exit limit of the bypass gas raised to 180 °C, the targets of the organic cycles fall by 6.2 to 6.6% and that of steam by 4.1%. In the cooler floor case, with the exit limit of the cooler exhaust lowered to 100 °C, the organic targets rise by 6.2 to 7.1% and that of steam by 3.3%. Steam responds less in both floor cases for two reasons. Its absorbed heat changes less than the available heat: it leaves 0.46 MW unrecovered at the cold end in the base case and part of the added heat in the cooler floor case. Its reoptimized drum pressure also rises in the bypass floor case and falls in the cooler floor case, so its thermal efficiency offsets more of the change in heat than those of the organic cycles do.

Enforcing the single-stage screening threshold of VFR $\leq$ 50 costs toluene 13.2% of its net power target: its evaporation pressure has to fall from 8.2 to 4.4 bar before the volume flow ratio meets the threshold. For steam, the threshold costs 1.4% of the target, and for supercritical cyclopentane no feasible design exists within the search domain in Table 2. For mixture A, the constrained design gives 9.29 MW at a volume flow ratio of 50, a penalty of 7.0% (Table 11), with the bubble temperature lowered from 208.5 to 189.0 °C and the evaporation pressure from 12.7 to 9.2 bar. Cyclohexane reaches 9.61 MW, the highest target under the threshold, a penalty of 7.9%, with the bubble temperature lowered from 215.7 to 192.3 °C and the evaporation pressure from 17.1 to 11.9 bar. Mixture B already meets the threshold at its base design, with a VFR of 39.

Figure 13 shows the design sweeps from which the retained designs are selected: the net power of the subcritical organic cycles against the bubble temperature, that of supercritical cyclopentane against the turbine inlet temperature and that of steam against

the superheat at drum pressures of 5 to 15 bar. For the organic cycles of Figure 13a,b, the shape of the sweep follows from which constraint has reached its limit. Below the optimum, the minimum approach is not binding: the working fluid absorbs the full source duty, and a higher bubble or turbine inlet temperature raises the cycle efficiency, so the net power rises. At the optimum, the approach at the limiting point also reaches its limit. Beyond the optimum, the working-fluid mass flow must fall to keep the minimum approach, so less heat is absorbed and the gain in efficiency no longer compensates for the loss of heat. The subcritical organic cycles reach their maximum net power at bubble temperatures of 205 to 216 °C. At a bubble temperature of 210 °C, above its optimum, toluene absorbs 37.74 MW and gives 9.73 MW.

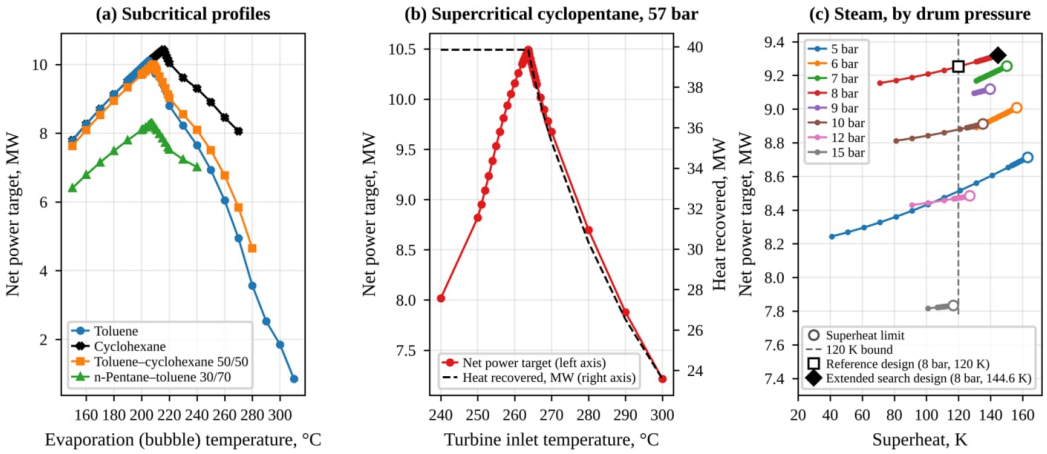

Figure 13. Design sweeps of the net power target: (**a**) subcritical organic cycles; (**b**) supercritical cyclopentane, with the heat recovered; (**c**) steam.

Supercritical cyclopentane reaches 10.49 MW at a turbine inlet temperature of 263.68 °C, and the sweep gives 9.94 MW at 258 °C and 9.90 MW at 268 °C, a sharp maximum. Below the optimum, cyclopentane still absorbs the full source duty, at a lower thermal efficiency. Above it, keeping the minimum approach at the 227 °C breakpoint reduces the admissible mass flow and heat uptake, the latter to 36.52 MW at 268 °C. The sharpness of the organic optima thus reflects how abruptly the active constraint changes at the limiting point: the source breakpoint for supercritical cyclopentane and the bubble point for the subcritical cycles.

The steam superheat curves of Figure 13c behave differently. At 8 bar and within the adopted 120 K bound, the designs of the search that meet the 0.88 limit on the turbine outlet quality have superheats of 71 to 120 K. Over this range, the minimum approach remains active, and increasing the superheat raises the net power modestly despite a small reduction in the absorbed heat. At the 120 K bound, the 8-bar design exceeds the 7- and 9-bar designs by 0.13 and 0.18 MW, respectively. Figure 13c also shows the curve of each drum pressure extended to its superheat limit, and at every plotted pressure the net power rises up to the limit. Across the drum pressures, the search finds its highest net power, 9.32 MW, at 8 bar with the superheat at its limit of 144.6 K. This is the extended search design in Table 7, 0.07 MW above the steam reference. Over the nine operating and constraint cases of Section 3.10 (Table 11), the gain of the extended search is 0.03 to 0.13 MW, and in no case does the extended search design change the nominal ranking of the fluids.

With the entrained dust of the preheater and bypass gases included, every base target rises by about 1.8% relative to its gas only value (Table 11), and the nominal ranking of the fluids is unchanged. The advantage of supercritical cyclopentane over cyclohexane changes from 0.063 to 0.064 MW, that of cyclohexane over toluene from 0.322 to 0.328 MW and that of toluene over mixture A from 0.108 to 0.110 MW. Because the dust raises all targets by

almost the same fraction, these differences change by at most 0.006 MW. The dust case was evaluated for the six base designs, not for the extended search design of steam.

Table 13 lists the sensitivity of the targets to the mixture compositions and the supercritical pressure, which Section 3.8 prescribes for the comparison. Each variant is placed again with the search procedure and constraints of the base designs, and the rows of mixtures A and B and of 1.25 p_{crit} are the base designs in Table 7. The composition sweep covers the compositions within the criteria of Section 3.8. The toluene–cyclohexane target falls from pure toluene to a shallow minimum of 9.87 MW at 70/30 to 80/20 and rises to 10.40 MW at 5/95 and 10.43 MW for pure cyclohexane. At cyclohexane mass fractions of 70% and above, the mixture exceeds toluene, by up to 0.29 MW at 5/95, as the composition approaches pure cyclohexane and the glide vanishes. For the n-pentane–toluene mixtures, the evaporation pressure reaches the adopted limit in Table 2 at n-pentane mass fractions of 50% and above. Every tested n-pentane–toluene composition lies 1.47 to 1.87 MW below toluene, the highest target being 8.64 MW at 50/50, and the 40/60 composition gains 0.17 MW over mixture B but would still rank last against the other five base designs. For mixture B, the evaporation lies about 100 K and 17 bar beyond the fitting data of the n-pentane–toluene binary interaction parameters, and for the other n-pentane–toluene compositions 10 to 29 bar above the highest fitted pressure (Section 4.5). No validation is available at these evaporation conditions, and the n-pentane–toluene results of this section are therefore extrapolated predictions of the mixture model.

Table 13. Effect of the mixture composition by mass and of the supercritical pressure on the base designs.

Variant	p_{evap} or p (bar)	T_{bubble} or T_4 (°C)	Glide (K)	$\dot{W}_{net}$ (MW)	η_{th} (%)	VFR	$\dot{E}_D$ (MW)	Limiting Approach (K)
Toluene	8.2	205.2	0	10.11	25.4	98	2.28	5.00
Toluene–cyclohexane 90/10	9.0	204.5	2.4	9.94	25.0	82	2.17	5.00
Toluene–cyclohexane 80/20	9.9	205.2	3.7	9.87	24.8	76	2.11	5.00
Toluene–cyclohexane 70/30	10.8	206.1	4.3	9.87	24.8	73	2.06	5.00
Toluene–cyclohexane 60/40	11.8	207.2	4.3	9.92	24.9	72	2.01	5.00
Toluene–cyclohexane 50/50 (A)	12.7	208.5	3.8	10.00	25.1	72	1.98	5.00
Toluene–cyclohexane 40/60	13.6	209.8	3.0	10.10	25.3	73	1.94	5.00
Toluene–cyclohexane 30/70	14.5	211.2	2.2	10.21	25.6	74	1.90	5.00
Toluene–cyclohexane 20/80	15.4	212.8	1.3	10.29	25.8	75	1.86	5.00
Toluene–cyclohexane 15/85	15.9	213.6	0.9	10.33	25.9	76	1.85	5.00
Toluene–cyclohexane 10/90	16.3	214.4	0.6	10.36	26.0	76	1.83	5.00
Toluene–cyclohexane 5/95	16.7	215.1	0.3	10.40	26.1	77	1.82	5.00
Cyclohexane	17.1	215.7	0	10.43	26.2	78	1.80	5.00
n-Pentane–toluene 10/90	11.4	202.3	14.8	8.49	21.3	42	1.92	5.00
n-Pentane–toluene 20/80	14.8	203.6	21.5	8.24	20.7	37	1.78	5.00
n-Pentane–toluene 30/70 (B)	18.6	207.3	23.4	8.28	20.8	39	1.72	5.00
n-Pentane–toluene 40/60	23.5	214.0	21.6	8.45	21.2	44	1.69	5.00
n-Pentane–toluene 45/55	26.8	219.3	19.3	8.56	21.5	49	1.67	5.00
n-Pentane–toluene 50/50	30.3	224.8	16.3	8.64	21.7	56	1.72	7.15
n-Pentane–toluene 55/45	30.3	220.5	15.3	8.57	21.5	54	1.95	12.03
n-Pentane–toluene 60/40	30.3	216.4	14.0	8.51	21.4	51	2.18	16.88
Cyclopentane, 1.10 p_{crit}	50.4	255.5	—	10.50	26.4	102	1.52	5.00
Cyclopentane, 1.25 p_{crit}	57.3	263.7	—	10.49	26.3	126	1.49	5.00
Cyclopentane, 1.40 p_{crit}	64.2	270.4	—	10.47	26.3	149	1.47	5.00

Varying the supercritical pressure changes the cyclopentane target by at most 0.03 MW, and the lower pressure of 1.10 p_{crit} gives almost the same power at a lower volume flow ratio, 102 against 126, still above the threshold.

Table 14 lists the sensitivity of the targets to the component efficiencies, varied one at a time in the retained designs with the procedure of Section 3.10. The pump efficiency is held at 0.65 during the turbine sweep and the turbine efficiency at 0.85 during the pump sweep, so that the 0.85 column reproduces the base design targets in Table 7. A common turbine efficiency of 0.80 or 0.90 changes every net power target by 0.39 to 0.67 MW per 5 percentage points of efficiency, whereas a pump efficiency of 0.60 or 0.70 changes a target by at most 0.07 MW. Since the achievable expander efficiency may differ between cycles whose volume flow ratios range from 39 to 126, the results for each fluid are also used to estimate, by linear interpolation between the computed turbine efficiencies of 0.80 and 0.85, the turbine efficiency at which each nominal power difference of Section 5.2 reaches zero. The 0.06 MW advantage of supercritical cyclopentane over cyclohexane is estimated to reach zero at a cyclopentane turbine efficiency near 0.845, about 0.5 percentage points below the 0.85 value of the other cycles. The 0.32 MW advantage of cyclohexane over toluene reaches zero at a cyclohexane turbine efficiency near 0.824, about 2.6 percentage points lower, and the 0.11 MW advantage of toluene over mixture A at a toluene turbine efficiency near 0.84, about 1 percentage point lower. The ranking of the retained designs is nominal, and the smaller differences are within the range that unequal expander efficiencies could reverse. The efficiencies are adopted values rather than measured quantities, so their effect is given as a sensitivity rather than as part of the measurement uncertainty.

Table 14. Effect of the turbine and pump isentropic efficiencies on the net power target (MW).

Cycle	$\eta_t = 0.80$	$\eta_t = 0.85$	$\eta_t = 0.90$	$\eta_p = 0.60$	$\eta_p = 0.70$
Cyclopentane, supercritical	9.82	10.49	10.97	10.42	10.55
Cyclohexane, subcritical	9.80	10.43	10.88	10.41	10.44
Toluene, subcritical	9.50	10.11	10.55	10.10	10.11
Toluene–cyclohexane 50/50 (A)	9.40	10.00	10.44	9.98	10.01
Steam	8.71	9.25	9.80	9.25	9.25
n-Pentane–toluene 30/70 (B)	7.78	8.28	8.68	8.26	8.30

The fluids are compared at a common condenser liquid outlet temperature of 40 °C. At this outlet, the mixtures condense with a minimum approach of 10 K at the cold end, twice the prescribed 5 K, whereas the pure fluids are close to it (Table 8). At the lowest condensing level allowed by the 5 K condenser approach (Table 15), the targets of the pure fluids therefore change by at most 0.01 MW, whereas mixture A gains 0.34 MW and mixture B 0.31 MW. Mixture A is then 0.23 MW above toluene, at a VFR raised to 90.5, and 0.10 MW below cyclohexane. For mixture B, a cooling-water temperature rise of 15 or 20 K adds nothing to this lowest-condensing-level design, since its minimum condenser approach stays at the cold end.

A working-fluid pressure drop of 0.2 bar costs at most 3.0 kW when the drop lies before the source exchangers, essentially the added pump power, and up to 103 kW, for toluene, when it lies after them (Table 16). With either location of the drop, the minimum approach remains associated with the same physical feature: the bubble point of the subcritical cycles, whose temperature rises by at most 1.4 K with the drop after the exchangers, and the 227 °C source breakpoint for supercritical cyclopentane, where the limiting fluid temperature does not move.

Table 15. Designs at the lowest condensing level allowed by the 5 K condenser approach.

Cycle	Liquid Outlet (°C)	p_{cond} (bar)	$\dot{W}_{net}$ (MW)	Change from Table 7 (kW)	VFR
Cyclopentane, supercritical	39.9	0.736	10.50	9.9	126.7
Cyclohexane, subcritical	39.9	0.245	10.44	7.3	77.9
Toluene, subcritical	39.9	0.079	10.11	5.5	98.9
Toluene–cyclohexane 50/50 (A)	35.0	0.148	10.34	340.2	90.5
Steam	40.0	0.074	9.25	0.0	55.9
n-Pentane–toluene 30/70 (B)	35.0	0.467	8.60	311.0	46.9
n-Pentane–toluene 30/70 (B), water rise 15 or 20 K	35.0	0.467	8.60	311.0	46.9

Table 16. Effect of a working-fluid pressure drop on the net power target and the limiting fluid temperature.

Cycle	$\Delta\dot{W}_{net}$, Loss Before the Exchangers (kW)		$\Delta\dot{W}_{net}$, Loss After the Exchangers (kW)		Rise of the Limiting Fluid Temperature at 0.2 bar (K)	
	0.1 bar	0.2 bar	0.1 bar	0.2 bar	Loss Before	Loss After
Cyclopentane, supercritical	−1.3	−2.7	−2.8	−5.9	0.00	0.00
Cyclohexane, subcritical	−1.4	−3.0	−24.1	−48.4	0.00	0.78
Toluene, subcritical	−1.2	−2.5	−51.3	−102.7	0.00	1.39
Toluene–cyclohexane 50/50 (A)	−1.2	−2.7	−32.3	−64.8	0.00	1.00
Steam	−0.2	−0.4	−38.9	−77.5	0.00	1.03
n-Pentane–toluene 30/70 (B)	−1.3	−2.7	−21.2	−42.7	0.00	0.78

When the mill-off designs are operated with the raw mill running and their cycle states held, every cycle absorbs the whole 34.06 MW surplus of the mill-on case at a recalculated mass flow. The organic cycles therefore lose 14.5% of their net power, the fraction of the heat removed, and the steam reference 13.5%, since it already left 0.46 MW unrecovered in the base case. The held designs lie 3.4 to 5.5% below the corresponding mill-on targets in Table 11 (Table 17).

Table 17. Mill-off designs operated with the raw mill on.

Cycle	Mill-Off Design			Mill-On Target, $\dot{W}_{net}$ (MW)
	$\dot{W}_{net}$, Mill Off (MW)	$\dot{W}_{net}$, Mill On (MW)	Change (%)	
Cyclopentane, supercritical	10.49	8.97	−14.5	9.44
Cyclohexane, subcritical	10.43	8.91	−14.5	9.43
Toluene, subcritical	10.11	8.64	−14.5	9.02
Toluene–cyclohexane 50/50 (A)	10.00	8.55	−14.5	8.90
Steam	9.25	8.00	−13.5	8.29
n-Pentane–toluene 30/70 (B)	8.28	7.08	−14.5	7.38

When the common turbine efficiency of 0.85 is replaced by stage-dependent estimates from the axial turbine correlation of Macchi and Astolfi [60] (Appendix A), cyclohexane gives the most power at one, two and three stages, 9.90, 10.45 and 10.64 MW, respectively. For supercritical cyclopentane, the estimates are 9.52, 10.28 and 10.53 MW, at a size parameter SP of 0.31 m and an isentropic volume ratio of 120, compared with 0.53 m and 75 for cyclohexane (Table A2). The ranking of the retained designs at the common turbine efficiency of 0.85 (Section 5.2) is therefore nominal. These estimates are screening values for axial turbines at optimized speed; the validation of the correlation for the present fluid conditions is limited, and the estimate for supercritical cyclopentane, at an inlet compressibility factor of 0.43, is the least certain.

Over all retained designs and designs of the sensitivity analysis, the highest turbine inlet temperatures of the organic working fluids are 218 to 272 °C, each reached in the mill-on case (Table 4). Their margins to the reported or adopted stability limits range from 28 K for supercritical cyclopentane to 220 K for cyclohexane.

5.7. Comparison with Published Cement Studies

For comparison with the cement studies reviewed in Section 1, the targets are expressed per tonne of clinker. The heat available above the cutoffs, 39.85 MW at a clinker production of 183 t/h, corresponds to 784 MJ per tonne of clinker, and the net power targets correspond to 57.3 kWh/t for supercritical cyclopentane, 57.0 kWh/t for cyclohexane, 55.2 kWh/t for toluene, 54.6 kWh/t for mixture A, 50.6 kWh/t for steam and 45.3 kWh/t for mixture B. For a 3800 t/d line, Khurana et al. [2] estimated a steam plant of 4.4 MW, about 28 kWh per tonne of clinker, which would cover about 30% of the electricity demand of that plant. The targets in Table 7 are not directly comparable with such plant estimates, for three reasons. First, they use all three exhaust streams above 150 °C rather than the preheater gas and the cooler exhaust alone. Second, they are set at a 5 K approach, the most optimistic of the three approaches tested, 5, 10 and 20 K. Third, they are thermodynamic upper bounds on the recovery that a heat exchanger network realizes with the evaluated cycles, as Section 5.3 shows.

The three studies closest in method use different boundaries. Mian et al. [27] applied pinch analysis and process integration to a process model of cement production, with the streams taken from the model rather than from a plant balance. Han et al. [28] applied pinch and exergy analysis to an operating steam waste-heat plant and obtained a theoretical gain of 7.6% and a measured gain of 5.0% in power generation; their analysis concerns the retrofit of an existing network rather than a target for a line. Mahmoud et al. [4] combined the kiln shell, preheater and cooler heat of a plant in a Kalina cycle and obtained 7.35 MW, against 6.86 MW for separate recovery. Their comparison concerns alternative recovery systems; the closest comparison here is that of the three source-exchanger arrangements with the composite targets (Section 5.3). These published results provide context rather than a comparison based on matched boundaries: the present values are shaft power targets before generator and auxiliary losses, and the studies differ in source boundaries and temperature constraints.

For the working-fluid comparison, Fergani et al. [17] placed cyclohexane–toluene and benzene–toluene mixtures on a single cement exhaust stream of 350 °C through an oil loop and reported benefits for selected optimized mixtures under their source and cycle conditions. The present study places the mixtures directly on the composite curve of three streams, at a fixed composition. In the present comparison with the common 40 °C condenser outlet, mixture A produces 1.1% less net power than toluene and mixture B 18.0% less, although both destroy less exergy in the source exchangers than toluene; at the lowest condensing level that keeps the 5 K condenser approach, mixture A lies 0.23 MW

above toluene (Section 5.6). Over the evaluated toluene–cyclohexane compositions, the target falls below that of toluene to a minimum near 70/30 to 80/20 and rises above it at cyclohexane mass fractions of 70% and above, to the highest value with pure cyclohexane (Section 5.6). For the supercritical cycle, Lai et al. [6] and the supercritical studies reviewed in Section 1 report the closer temperature match as its advantage. On a measured cement source, the present study gives the corresponding comparison, in which the fluid and the regime change together: supercritical cyclopentane at 57 bar gives 0.39 MW more than subcritical toluene, with the lowest exergy destruction of the set and a limiting approach fixed by a breakpoint of the source. Over subcritical cyclohexane at 17.1 bar, its advantage is a nominal 0.06 MW (Section 5.8). For the steam reference, Karellas et al. [1] compared steam and ORC by energy and exergy analysis and found steam more efficient for exhaust gases above 310 °C; here, only the cooler exhaust exceeds that temperature, and 62% of the source heat lies between 150 and 227 °C (Section 5.1). Kizilkan [30] compared steam with supercritical carbon dioxide on a cement plant. Neither study placed the cycles on a composite curve of measured streams.

5.8. Practical Implications for the Cement Line

For the line studied, the three exhaust streams offer net power targets of 10.1 to 10.5 MW for the three organic fluids of highest power, supercritical cyclopentane, cyclohexane and toluene, at a 5 K approach and 9.3 to 9.7 MW at 20 K. Running the raw mill, which raises the exit limit of the preheater gas to 202 °C, reduces the targets of the working fluids by 9.6 to 10.9%. In the 5 K approach, the three highest targets lie within about 4% of each other, and this spread is to be weighed with the pressure level, the condensing conditions and the expander requirements in the subsequent selection of the equipment. Supercritical cyclopentane gives the highest target and condenses near atmospheric pressure, but it operates at 57 bar and has a VFR of 126, well above the single-stage screening threshold. Cyclohexane is a nominal 0.06 MW lower at 17.1 bar, with a condensing pressure of 0.25 bar and a VFR of 78, and toluene 0.39 MW lower at 8.2 bar, with a condensing pressure of 0.08 bar and a VFR of 98. According to the efficiency sensitivity in Table 14, these differences are estimated to vanish at a cyclopentane turbine efficiency about 0.5 percentage points lower against cyclohexane and about 3 percentage points lower against toluene. The sign of the difference between the two highest targets is not resolved under the adopted measurement bounds: the $k = 2$ interval of the difference between supercritical cyclopentane and cyclohexane crosses zero, whereas the intervals of their differences from toluene do not (Table A3).

Among the base designs without the VFR constraint, the mixture B design is the only one below the screening threshold of 50, at a target 21% below that of supercritical cyclopentane. Under the threshold, toluene, mixture A and cyclohexane give 8.77, 9.29 and 9.61 MW, respectively, whereas no feasible supercritical cyclopentane design exists within the search domain in Table 2, so its target remains flagged for further expander assessment in this comparison. In the base case, the steam reference, at the adopted upper superheat bound, has a target of 9.25 MW, with the lowest turbine mass flow and a working fluid free of the decomposition and flammability limits of the organic fluids. Supercritical cyclopentane exceeds the 9.32 MW of the extended search design of steam by 1.17 MW. For the steam reference, the 0.46 MW of unrecovered source heat and the 3.10 MW of exergy destroyed in the source exchangers are the losses that the organic cycles reduce.

In the modeled case, removing the excess false air raises the reoptimized net power targets by a nominal 0.09 to 0.14 MW on the consistent basis, and the nominal ranking of the cycles is unchanged in both false air cases. False air reduction addresses the fuel demand of heating the ingressed air, and under the modeled removal assumptions it leaves the heat recovery opportunity largely intact; heat recovery and false air reduction are therefore

complementary measures. Lowering the cooler exhaust cutoff from 150 to 100 °C raises the targets of the organic cycles by 6.2 to 7.1%. The composite targets define the recovery that the cement line can approach, and how closely a recovery plant approaches them depends on its exchanger network and on its operation. In the series arrangement, the working fluids absorb 83 to 89% of the composite heat targets at the retained mass flow, whereas in the idealized split-flow arrangement they reach the retained turbine inlet state at 99.8 to 100% of that flow (Section 5.3). When a mill-off design is operated with the raw mill running and its cycle states held, the working fluid reaches the turbine inlet state only at a reduced flow, and the mill-on target indicates what retuning the operating point of such a design could gain (Section 5.6). For such retuning, Wu et al. [65] simulated an ORC on cement exhaust with the superheat held by the pump speed and the evaporation pressure by the expander speed and with feedforward from the gas temperature and flow. Hu et al. [66] compared control strategies for the off-design operation of an ORC, including sliding pressure and inlet guide vanes, which adapt its operating point to the heat supplied.

6. Conclusions

The net power targets of this study are nominal values of net shaft power under the adopted assumptions and thermodynamic upper bounds for the evaluated cycles on this source. The three exhaust streams of the cement line, the preheater exit gas, the bypass gas after its quench and the cooler exhaust, offer 39.85 MW of heat and 15.49 MW of exergy above the adopted 150 °C cutoff in the base case with the raw mill stopped. Within the boundary of these selected streams, the heat cascade is surplus only, with the pinch at the top and no hot utility. The composite curve changes slope at the supply temperatures of the streams, and 62% of the heat lies in the interval from 150 to 227 °C, where all three contribute. Temperature matching within that interval is therefore an important determinant of the recovery potential.

At a minimum approach of 5 K, the net power targets are 10.49 MW for supercritical cyclopentane, 10.43 MW for cyclohexane, 10.11 MW for toluene, 10.00 MW for the toluene–cyclohexane mixture of 50/50 by mass, 9.25 MW for the steam reference and 8.28 MW for the n-pentane–toluene mixture of 30/70 by mass, at thermal efficiencies from 20.8% for the n-pentane–toluene mixture to 26.3% for supercritical cyclopentane. The evaporation of the n-pentane–toluene mixture lies about 100 K and 17 bar beyond the fitting data of its binary interaction parameters, where no validation is available, so the results of this mixture are extrapolated predictions of the mixture model. Extending the steam superheat search beyond its 120 K bound to the superheat limit set by the source, 144.6 K at 8 bar, raises the steam target to 9.32 MW, and the advantage of supercritical cyclopentane over this steam design is 1.17 MW rather than 1.24 MW. In the six base designs, the minimum approach is reached at the bubble point for the subcritical cycles and at the 227 °C breakpoint of the source for supercritical cyclopentane, the only one of these designs whose limiting location is set by the source rather than by a phase change.

The exergy destroyed in the source exchangers, 1.49 MW for supercritical cyclopentane against 3.10 MW for steam, measures the temperature match, whereas the net power measures the performance of the whole cycle. The heating curve of the n-pentane–toluene mixture follows the composite with an evaporation glide of 23.4 K, and the mixture destroys less exergy than toluene, but it produces 18.0% less power. It also condenses over a glide of 38.4 K against the 5 K rise of the cooling water, a mismatch consistent with the mechanisms reported for zeotropic cycles; the contribution of this mismatch to the power difference is not isolated here. A close temperature match in the source exchangers is thus not by itself a guarantee of the highest power, and the exergy destruction is read together with the net power. The common condenser outlet also bears on the mixture comparison: at the lowest

condensing level that keeps the 5 K condenser approach, the toluene–cyclohexane mixture lies 0.23 MW above toluene and 0.10 MW below cyclohexane.

With the three source exchangers in series, the working fluid absorbs 83 to 89% of the composite heat targets at the retained mass flow, since the cooler exhaust meets the fluid last and leaves part of its heat above the cutoff. At the retained cycle states, the fluid then reaches the turbine inlet state only at a reduced flow, at which the net power is 6.48 to 8.46 MW, highest for toluene. In an idealized two-section split-flow arrangement, the working fluid reaches the inlet state at 99.8 to 100% of the target mass flow, and the net power comes within 0.2% of its target. Raising the prescribed approach from 5 to 20 K reduces the targets by 7.7 to 8.8% and leaves the nominal ranking unchanged at the tested approaches. With the raw mill running and the cycle states retained, net power falls by 14.5% for the organic cycles and 13.5% for the steam reference, since the admissible mass flow is recalculated for the reduced heat. Reoptimizing the cycles for raw mill operation limits the reduction to 9.6 to 10.9% of the corresponding mill-off targets. A cooler exhaust cutoff of 100 °C raises the organic targets by 6.2 to 7.1%. The raw mill mode and the cooler exhaust cutoff are therefore important operating conditions for the recovery assessment.

Including the entrained dust raises every net power target by about 1.8% without changing the nominal ranking, and the differences among the three highest targets change by less than 0.01 MW. Among the tested binary compositions, the targets differ from those of the prescribed compositions by up to 0.40 MW for toluene–cyclohexane and 0.36 MW for n-pentane–toluene, whose maximum lies at the adopted pressure limit. At cyclohexane mass fractions of 70% and above, the toluene–cyclohexane mixture exceeds toluene, and pure cyclohexane gives the highest target of the pair; the supercritical pressure changes the cyclopentane target by at most 0.03 MW. With the comparator held at the turbine efficiency of 0.85, the advantage of supercritical cyclopentane over cyclohexane is estimated to vanish at a cyclopentane turbine efficiency about 0.5 percentage points lower, and the advantage of cyclohexane over toluene is estimated to vanish at a cyclohexane turbine efficiency about 2.6 percentage points lower. The ranking of the retained designs is therefore nominal. Across the retained and sensitivity designs, the highest turbine inlet temperatures of the organic working fluids are 28 to 220 K below their reported or adopted thermal stability limits.

At the common turbine efficiency of 0.85 and the 40 °C condenser outlet, supercritical cyclopentane and cyclohexane give the two highest nominal net power targets. The measurement bounds adopted for the plant balance inputs propagate to standard uncertainties of 0.28 to 0.38 MW, or 3.1 to 3.6% of the targets, in the retained designs. Under these bounds, the $k = 2$ intervals of the paired differences of supercritical cyclopentane and cyclohexane from toluene exclude zero, whereas that of the paired difference between the two crosses zero, so its sign is not resolved.

Among the base designs without the VFR constraint, only the design with the n-pentane–toluene mixture lies below the single-stage screening threshold, a volume flow ratio of 50; the other organic cycles exceed it at the common 40 °C condenser outlet and are flagged for further expander assessment. Under the threshold of VFR ≤ 50 and at the common efficiency, cyclohexane gives the highest target, 9.61 MW, 7.9% below its target without the threshold, and the toluene–cyclohexane mixture reaches 9.29 MW, 7.0% below its corresponding target. In a separate comparison, the common turbine efficiency of 0.85 is replaced by stage-dependent screening estimates from the correlation of Macchi and Astolfi [60]; for one, two and three axial turbine stages, cyclohexane then has the highest estimated net power.

The removable false air of the preheater, 5983 Nm^3/h on the consistent basis, that is, on the inlet basis of the oxygen balance, is heated by the kiln fuel and carries about 0.57 MW of sensible enthalpy above ambient at the measured exit temperature. In the modeled case,

in which the heat that warmed this air stays in the remaining gas rather than being saved as kiln fuel, removing it raises the preheater exit temperature from 289.5 to 294.5 °C and the reoptimized targets by a nominal 0.09 to 0.14 MW, about 1% of the targets. In the fixed designs, the paired gain from the removal is +0.05 to +0.09 MW, and its k = 2 intervals cross zero for the organic cycles but not for the steam reference. The nominal ranking of the cycles is unchanged in both false air cases. False air reduction addresses the fuel demand of heating the ingressed air, and under the modeled removal assumptions it leaves the heat recovery opportunity largely intact, so heat recovery and false air reduction are complementary measures; false air reduction remains primarily a fuel-saving measure.

Funding: The research work was funded by the Deanship of Scientific Research (DSR) at King Abdulaziz University, Jeddah, Saudi Arabia, under grant no. IPP: 1016-829-2026. The author, therefore, acknowledges with thanks DSR for technical and financial support.

Data Availability Statement: The measured heat balance data used in this study are available from the author on reasonable request, subject to the confidentiality conditions of the plant.

Acknowledgments: The research work was funded by the Deanship of Scientific Research (DSR) at King Abdulaziz University, Jeddah, Saudi Arabia, under grant no. IPP: 1016-829-2026. The author, therefore, acknowledges with thanks DSR for technical and financial support. Duringthe preparation of this work, the author used ChatGPT (GPT-6 Extra, OpenAI) and Claude (Claude Fable 5.1, Anthropic) in order to improve readability and language, to verify numerical and structural consistency and to improve the graphics of the schematic diagrams. After using these tools/services, the author reviewed and edited the content as needed and takes full responsibility for the content of the published article.

Conflicts of Interest: The author declares no conflicts of interest.

Nomenclature

Symbol	Description	Unit
a_i	Half-width of the rectangular uncertainty distribution of input i	units of x_i
A_i	Coefficients of the turbine correlation, Equation (A1)	—
c_p	Isobaric specific heat of the wet gas	kJ/(kg K)
$\overline{c}_{p,i}$	Molar isobaric heat capacity of species i	kJ/(kmol K)
D	Paired difference between two net power targets	MW
$\dot{E}$	Exergy flow rate	MW
F_i	Terms of the turbine correlation, Equation (A1)	—
H	Heat released by the composite above a temperature	MW
h	Specific enthalpy	kJ/kg
$\overline{h}$	Specific enthalpy above the ambient temperature	kJ/kg
M	Molar mass	kg/kmol
$\dot{m}$	Mass flow rate	kg/s
p	Pressure	bar
$\dot{Q}$	Heat flow rate	MW
q	Heat counted from the hot end of the composite curve	MW
q_{in}	Heat taken by one kilogram of working fluid	kJ/kg
q_c	Heat rejected per kilogram of working fluid, counted from the condenser liquid outlet	kJ/kg
q_{cond}	Condenser duty per kilogram of working fluid	kJ/kg
R	A target quantity	units of the target
R_k	Cascade heat surplus below interval k	MW
r	False air volume per volume of gas entering the tower	—
s	Specific entropy	kJ/(kg K)
SP	Size parameter of the turbine	m

T	Temperature	°C, K
T^*	Shifted temperature	°C
u	Standard uncertainty	units of the quantity
$\dot{V}$	Volume flow rate at normal conditions	Nm^3/h
v	Specific volume	m^3/kg
VFR	Volume flow ratio across the turbine	—
V_r	Isentropic volume ratio of the turbine	—
$\dot{W}$	Power	MW
$\dot{W}_0$, $\dot{W}_1$	Net power targets with the measured preheater exit stream and with the removable false air taken out	MW
x_w	Moisture content of the gas by volume	—
x_5	Vapor quality at the turbine outlet	—
y_i	Mole fraction of species i	—
Z	Compressibility factor	—
z_j	Fraction of the working-fluid mass flow passing stage j	—
Greek symbols		
β	Isobaric expansion coefficient of the liquid	1/K
ΔH_k	Net heat of temperature interval k	MW
Δp	Working-fluid pressure drop	bar
ΔT_{min}	Minimum approach in the source exchangers	K
ΔT_{cond}	Prescribed minimum approach in the condenser	K
ΔT_{rec}	Recuperator cold-end approach	K
ΔT_{sh}	Steam superheat above the saturation temperature at the drum pressure	K
η_p, η_t	Isentropic efficiency of the pump and the turbine	—
η_{th}	Thermal efficiency of the cycle	—
η_{II}	Second law efficiency, net power over the exergy given up by the source	—
η_{conv}	Conversion efficiency, net power over the exergy taken up by the fluid	—
ρ	Normal density	kg/Nm^3
Subscripts		
0	Dead state	
1 to 6	Cycle state points of Figure 2	
A, B, C	Preheater exit gas, bypass gas, cooler exhaust	
al	Airlift blower air	
amb	Ambient	
bubble, dew	Bubble point, dew point	
cond	Condenser	
crit	Critical	
cw	Cooling water	
d	Entrained dust; dry, in Equation (24)	
D	Destroyed	
dry, wet	Dry gas, wet gas	
evap	Evaporation	
f	Exit limit	
fa	False air	
g	Gas without the excess false air	
HFO	Heavy fuel oil	
hs	Heat source of the validation benchmark	
hot	Hot composite	
in, out	Inlet, outlet	
j	Source exchanger (stage) j	
max	Maximum	
min	Minimum	

s	Stream; supply, in T_s
sat	Saturation
sh	Superheat
src	Source
wf	Working fluid
Abbreviations	
GCC	Grand composite curve
ORC	Organic Rankine cycle
VLE	Vapor–liquid equilibrium

Appendix A

Appendix A.1. Split-Flow Heat Allocation

Table A1 gives the allocation of the idealized two-section split-flow arrangement of Section 5.3 for each fluid. It lists the section boundary as the working-fluid state, given by the fluid temperature and the vapor quality and, for supercritical cyclopentane, which does not evaporate, by the temperature alone. For each exchanger, it lists the section, the stream, the fraction of the working-fluid mass flow, the duty, the gas inlet and outlet temperatures, and the minimum approach; the fractions of each section sum to one. The superheater of the steam cycle, on the cooler exhaust, takes the whole steam flow. The exchangers in Table A1 and their connections are those drawn in Figure 9c.

Table A1. Heat allocation in the split-flow arrangement.

Cycle	Section Boundary		Section	Stream	Fraction of the Working-Fluid Mass Flow	Duty (MW)	Gas Inlet → Outlet (°C)	Minimum Approach (K)
	T (°C)	Vapor Quality						
Toluene, subcritical	205.2	0.26	Upper	A	0.470	7.20	289.5 → 226.9	21.72
			Upper	C	0.530	8.12	320.0 → 227.0	21.84
			Lower	A	0.351	8.60	226.9 → 150.0	5.03
			Lower	B	0.380	9.31	227.0 → 150.0	5.00
			Lower	C	0.270	6.62	227.0 → 150.0	5.00
Cyclohexane, subcritical	215.7	0.12	Upper	A	0.470	7.20	289.5 → 226.9	11.18
			Upper	C	0.530	8.11	320.0 → 227.1	11.31
			Lower	A	0.350	8.59	226.9 → 150.1	5.00
			Lower	B	0.380	9.31	227.0 → 150.0	5.01
			Lower	C	0.270	6.62	227.1 → 150.0	5.06
Toluene–cyclohexane 50/50 (A)	209.2	0.22	Upper	A	0.470	7.20	289.5 → 226.9	17.66
			Upper	C	0.530	8.12	320.0 → 227.0	17.78
			Lower	A	0.351	8.60	226.9 → 150.0	5.01
			Lower	B	0.380	9.31	227.0 → 150.0	5.00
			Lower	C	0.270	6.62	227.0 → 150.0	5.00
n-Pentane–toluene 30/70 (B)	213.8	0.24	Upper	A	0.470	7.20	289.5 → 226.9	13.07
			Upper	C	0.530	8.12	320.0 → 227.0	13.19
			Lower	A	0.351	8.60	226.9 → 150.0	5.01
			Lower	B	0.380	9.31	227.0 → 150.0	5.00
			Lower	C	0.270	6.62	227.0 → 150.0	5.00

Table A1. *Cont.*

Cycle	Section Boundary		Section	Stream	Fraction of the Working-Fluid Mass Flow	Duty (MW)	Gas Inlet → Outlet (°C)	Minimum Approach (K)
	T (°C)	Vapor Quality						
Cyclopentane, supercritical	222.0	—	Upper	A	0.469	7.17	289.5 → 227.2	5.06
			Upper	C	0.531	8.12	320.0 → 227.0	5.00
			Lower	A	0.351	8.61	227.2 → 150.2	5.22
			Lower	B	0.379	9.29	227.0 → 150.2	5.05
			Lower	C	0.269	6.59	227.0 → 150.2	5.00
Steam	170.4	0.55	Super-heater	C	1.000	0.33	320.0 → 316.3	29.59
			Upper	A	0.510	8.13	289.5 → 218.7	10.37
			Upper	C	0.490	7.82	316.3 → 226.7	37.15
			Lower	A	0.313	7.22	218.7 → 154.0	5.00
			Lower	B	0.403	9.31	227.0 → 150.0	5.00
			Lower	C	0.284	6.57	226.7 → 150.2	5.00

Appendix A.2. Axial Turbine Efficiency Estimates

The turbine efficiencies of Section 5.6 are those of the correlation of Macchi and Astolfi [60] for one-, two- and three-stage axial turbines at optimized rotational speed,

$$\eta_t = \sum_{i=0}^{15} A_i F_i(\mathrm{SP},\, V_r) \tag{A1}$$

where SP, the size parameter, is the square root of the volume flow at the isentropic turbine outlet divided by the fourth root of the isentropic enthalpy drop, in m, and V_r is the ratio of that isentropic outlet volume flow to the inlet volume flow; it differs from the VFR of Equation (22), which is taken at the actual turbine outlet. The sixteen terms F_i are 1, the first to fourth powers of ln SP and of ln V_r, V_r itself, which the correlation for one stage omits, and six products of powers of ln V_r and ln SP; the terms and their coefficients, A_i, for one, two and three stages are given in [60]. The correlation is applied to the five organic cycles, whose size parameters and volume ratios lie within the stated ranges of 0.02 to 1 m and 1.2 to 200. SP depends on the mass flow and the mass flow on the efficiency, so SP, the efficiency and the mass flow are updated together until they are consistent in each design. The cycle states and the mass flow are recomputed by the placement of Equation (9), as for the efficiency sensitivity of Section 3.10. Table A2 gives SP and V_r in the retained designs. V_r, set by the retained turbine inlet state and condensing pressure, is the same in the estimates for one, two and three stages, and the converged SP differs from the tabulated value by less than 0.5%. The table also gives the compressibility factor at the turbine inlet Z_4 and the efficiencies and net power for one, two and three stages.

Appendix A.3. Uncertainty of the Net Power Differences

Table A3 gives the differences between the three highest net power targets in the retained designs, propagated as paired differences by Equation (27) under the measurement bounds of Section 3.10, with their standard uncertainties and k = 2 intervals. Each row subtracts the target of the second design named from that of the first, and an interval that includes zero leaves the sign of the difference unresolved.

Table A2. Axial turbine efficiency and estimated net power of the five organic fluids for one, two and three stages.

Cycle	SP (m)	V_r	Z_4	One Stage		Two Stages		Three Stages	
				η_t	$\dot{W}_{net}$ (MW)	η_t	$\dot{W}_{net}$ (MW)	η_t	$\dot{W}_{net}$ (MW)
Toluene, subcritical	0.851	93.7	0.83	0.796	9.46	0.848	10.08	0.868	10.27
Cyclohexane, subcritical	0.528	74.6	0.72	0.808	9.90	0.853	10.45	0.873	10.64
Toluene–cyclohexane 50/50 (A)	0.600	69.1	0.77	0.811	9.53	0.855	10.04	0.876	10.23
n-Pentane–toluene 30/70 (B)	0.367	37.6	0.71	0.830	8.08	0.867	8.42	0.888	8.58
Cyclopentane, supercritical	0.310	120.1	0.43	0.778	9.52	0.834	10.28	0.854	10.53

Table A3. Differences between the three highest net power targets and their uncertainties.

Difference	$\dot{W}_{net}$ Difference (MW)	u (MW)	$k = 2$ Interval (MW)
Cyclopentane−cyclohexane	0.063	0.071	−0.078 to +0.204
Cyclohexane−toluene	0.322	0.040	+0.243 to +0.402
Cyclopentane−toluene	0.385	0.072	+0.242 to +0.528

References

1. Karellas, S.; Leontaritis, A.-D.; Panousis, G.; Bellos, E.; Kakaras, E. Energetic and exergetic analysis of waste heat recovery systems in the cement industry. *Energy* **2013**, *58*, 147–156. [CrossRef]
2. Khurana, S.; Banerjee, R.; Gaitonde, U. Energy balance and cogeneration for a cement plant. *Appl. Therm. Eng.* **2002**, *22*, 485–494. [CrossRef]
3. Kasaeian, A.; Afshari, F.; Mahmoudkhani, M.; Masoumi, A.; Esmaeili Bidhendi, M. Waste heat recovery by thermodynamic cycles in cement plants: A review. *Energy* **2025**, *314*, 134087. [CrossRef]
4. Mahmoud, E.S.; Rady, M.; Abuhabaya, A.A.; Elsamahy, A.A. Separate and combined integration of Kalina cycle for waste heat recovery from a cement plant. *Therm. Sci.* **2022**, *26*, 1907–1925. [CrossRef]
5. Lanzerstorfer, C. Residue from the chloride bypass de-dusting of cement kilns: Reduction of the chloride content by air classification for improved utilisation. *Process Saf. Environ. Prot.* **2016**, *104*, 444–450. [CrossRef]
6. Lai, N.A.; Wendland, M.; Fischer, J. Working fluids for high-temperature organic Rankine cycles. *Energy* **2011**, *36*, 199–211. [CrossRef]
7. Drescher, U.; Brüggemann, D. Fluid selection for the organic Rankine cycle (ORC) in biomass power and heat plants. *Appl. Therm. Eng.* **2007**, *27*, 223–228. [CrossRef]
8. Shu, G.; Li, X.; Tian, H.; Liang, X.; Wei, H.; Wang, X. Alkanes as working fluids for high-temperature exhaust heat recovery of diesel engine using organic Rankine cycle. *Appl. Energy* **2014**, *119*, 204–217. [CrossRef]
9. Andreasen, J.G.; Larsen, U.; Knudsen, T.; Pierobon, L.; Haglind, F. Selection and optimization of pure and mixed working fluids for low grade heat utilization using organic Rankine cycles. *Energy* **2014**, *73*, 204–213. [CrossRef]
10. Liu, Q.; Duan, Y.; Yang, Z. Effect of condensation temperature glide on the performance of organic Rankine cycles with zeotropic mixture working fluids. *Appl. Energy* **2014**, *115*, 394–404. [CrossRef]
11. Shahrooz, M.; Lundqvist, P.; Nekså, P. Performance of binary zeotropic mixtures in organic Rankine cycles (ORCs). *Energy Convers. Manag.* **2022**, *266*, 115783. [CrossRef]
12. Raksa-in, W.; Duangduean, S.; Schulz, E.; Koonsrisuk, A. Resolving performance contradictions in ORC and alternative power cycles: Systematic analysis of five technologies with time-adjusted economic insights. *Energy* **2025**, *324*, 136130. [CrossRef]
13. Invernizzi, C.M.; Iora, P.; Manzolini, G.; Lasala, S. Thermal stability of n-pentane, cyclo-pentane and toluene as working fluids in organic Rankine engines. *Appl. Therm. Eng.* **2017**, *121*, 172–179. [CrossRef]
14. Ginosar, D.M.; Petkovic, L.M.; Guillen, D.P. Thermal stability of cyclopentane as an organic Rankine cycle working fluid. *Energy Fuels* **2011**, *25*, 4138–4144. [CrossRef]
15. Pasetti, M.; Invernizzi, C.M.; Iora, P. Thermal stability of working fluids for organic Rankine cycles: An improved survey method and experimental results for cyclopentane, isopentane and n-butane. *Appl. Therm. Eng.* **2014**, *73*, 764–774. [CrossRef]
16. Fergani, Z.; Touil, D.; Morosuk, T. Multi-criteria exergy based optimization of an organic Rankine cycle for waste heat recovery in the cement industry. *Energy Convers. Manag.* **2016**, *112*, 81–90. [CrossRef]

17. Fergani, Z.; Morosuk, T.; Touil, D. Exergy-based multi-objective optimization of an organic Rankine cycle with a zeotropic mixture. *Entropy* **2021**, *23*, 954. [CrossRef] [PubMed]
18. Kemp, I.C. *Pinch Analysis and Process Integration: A User Guide on Process Integration for the Efficient Use of Energy*, 2nd ed.; Butterworth-Heinemann: Oxford, UK, 2007.
19. Townsend, D.W.; Linnhoff, B. Heat and power networks in process design. Part I: Criteria for placement of heat engines and heat pumps in process networks. *AIChE J.* **1983**, *29*, 742–748. [CrossRef]
20. Chen, Q.; Xu, J.; Chen, H. A new design method for organic Rankine cycles with constraint of inlet and outlet heat carrier fluid temperatures coupling with the heat source. *Appl. Energy* **2012**, *98*, 562–573. [CrossRef]
21. Ryms, M.; Pyś, T.; Klugmann-Radziemska, E. Adapting the pinch point analysis to improve the ORC design process. *Int. J. Energy Res.* **2014**, *38*, 29–40. [CrossRef]
22. Sarkar, J. Novel pinch point method based exergetic optimisation of subcritical organic Rankine cycle for waste heat recovery. *Int. J. Exergy* **2018**, *25*, 281–299. [CrossRef]
23. Manalac, E.J.; Berana, M.S.; Kim, S.C. Performance analysis of cement plant waste-heat recovery for power generation based on partial evaporating cycle with ejector. *Energy Technol.* **2025**, *13*, 2401419. [CrossRef]
24. Stijepović, M.Z.; Papadopoulos, A.I.; Linke, P.; Grujić, A.S.; Seferlis, P. An exergy composite curves approach for the design of optimum multi-pressure organic Rankine cycle processes. *Energy* **2014**, *69*, 285–298. [CrossRef]
25. Yong, J.Y.; Nemet, A.; Varbanov, P.S.; Klemeš, J.J.; Čuček, L.; Kravanja, Z.; Mantelli, V. Heat exchanger network modification for waste heat utilisation under varying feed conditions. *Chem. Eng. Trans.* **2015**, *43*, 1279–1284. [CrossRef]
26. Lee, J.-Y.; Chen, P.-L.; Xie, P.-S.; Bandyopadhyay, S. Design of multi-cycle organic Rankine cycle systems for low-grade heat utilisation. *Energy* **2024**, *310*, 133252. [CrossRef]
27. Mian, A.; Bendig, M.; Piazzesi, G.; Manente, G.; Lazzaretto, A.; Maréchal, F. Energy integration in the cement industry. *Comput. Aided Chem. Eng.* **2013**, *32*, 349–354. [CrossRef]
28. Han, T.; Wang, C.; Zhu, C.; Che, D. Optimization of waste heat recovery power generation system for cement plant by combining pinch and exergy analysis methods. *Appl. Therm. Eng.* **2018**, *140*, 334–340. [CrossRef]
29. Wang, J.; Dai, Y.; Gao, L. Exergy analyses and parametric optimizations for different cogeneration power plants in cement industry. *Appl. Energy* **2009**, *86*, 941–948. [CrossRef]
30. Kizilkan, O. Performance assessment of steam Rankine cycle and sCO2 Brayton cycle for waste heat recovery in a cement plant: A comparative study for supercritical fluids. *Int. J. Energy Res.* **2020**, *44*, 12329–12343. [CrossRef]
31. Sanaye, S.; Khakpaay, N.; Chitsaz, A.; Yahyanejad, M.H.; Zolfaghari, M. A comprehensive approach for designing, modeling and optimizing of waste heat recovery cycle and power generation system in a cement plant: A thermo-economic and environmental assessment. *Energy Convers. Manag.* **2020**, *205*, 112353. [CrossRef]
32. Amarasinghe, W.S.; Husum, I.; Tokheim, L.-A. Waste heat availability in the raw meal department of a cement plant. *Case Stud. Therm. Eng.* **2018**, *11*, 1–14. [CrossRef]
33. Akroot, A.; Ameen, K.A.; Ibrahim, H.M.; Wahhab, H.A.A.; Chaichan, M.T. Modelling and analysis of enhanced power generation by recovering waste heat from Fallujah White Cement Factory for clean energy sustainability. *Energy Eng.* **2026**, *123*, 22. [CrossRef]
34. Khafajah, H.I.; Abdelsamie, M.M.; Ali, M.I.H. Thermoeconomic assessment of a cement-plant waste-heat-driven trigeneration system for power, cooling, and desalination. *Energy Nexus* **2026**, *21*, 100631. [CrossRef]
35. Hughes, S.; Cvetic, P.; Newby, R.; Homsy, S.; Zoelle, A.; Woods, M.; Grol, E.; Fout, T. The impact of cement plant air ingress on membrane-based CO2 capture retrofit cost. *Carbon Capture Sci. Technol.* **2024**, *11*, 100201. [CrossRef]
36. Bejan, A. *Advanced Engineering Thermodynamics*, 4th ed.; John Wiley & Sons: Hoboken, NJ, USA, 2016.
37. Bell, I.H.; Wronski, J.; Quoilin, S.; Lemort, V. Pure and pseudo-pure fluid thermophysical property evaluation and the open-source thermophysical property library CoolProp. *Ind. Eng. Chem. Res.* **2014**, *53*, 2498–2508. [CrossRef] [PubMed]
38. Irungu, S.N.; Muchiri, P.; Byiringiro, J.B. The generation of power from a cement kiln waste gases: A case study of a plant in Kenya. *Energy Sci. Eng.* **2017**, *5*, 90–99. [CrossRef]
39. Linnhoff, B.; Flower, J.R. Synthesis of heat exchanger networks: I. Systematic generation of energy optimal networks. *AIChE J.* **1978**, *24*, 633–642. [CrossRef]
40. Kotas, T.J. *The Exergy Method of Thermal Plant Analysis*; Krieger Publishing: Malabar, FL, USA, 1995.
41. Braimakis, K.; Karellas, S. Integrated thermoeconomic optimization of standard and regenerative ORC for different heat source types and capacities. *Energy* **2017**, *121*, 570–598. [CrossRef]
42. Lecompte, S.; Huisseune, H.; van den Broek, M.; De Paepe, M. Methodical thermodynamic analysis and regression models of organic Rankine cycle architectures for waste heat recovery. *Energy* **2015**, *87*, 60–76. [CrossRef]
43. Mago, P.J.; Srinivasan, K.K.; Chamra, L.M.; Somayaji, C. An examination of exergy destruction in organic Rankine cycles. *Int. J. Energy Res.* **2008**, *32*, 926–938. [CrossRef]
44. Macchi, E.; Perdichizzi, A. Efficiency prediction for axial-flow turbines operating with nonconventional fluids. *J. Eng. Power* **1981**, *103*, 718–724. [CrossRef]

45. Zhai, H.; An, Q.; Shi, L.; Lemort, V.; Quoilin, S. Analysis of the quantitative correlation between the heat source temperature and the critical temperature of the optimal pure working fluid for subcritical organic Rankine cycles. *Appl. Therm. Eng.* **2016**, *99*, 383–391. [CrossRef]
46. White, M.T.; Sayma, A.I. Simultaneous cycle optimization and fluid selection for ORC systems accounting for the effect of the operating conditions on turbine efficiency. *Front. Energy Res.* **2019**, *7*, 50. [CrossRef]
47. Bell, I.H.; Lemmon, E.W. Automatic fitting of binary interaction parameters for multi-fluid Helmholtz-energy-explicit mixture models. *J. Chem. Eng. Data* **2016**, *61*, 3752–3760. [CrossRef]
48. Zühlsdorf, B.; Jensen, J.K.; Cignitti, S.; Madsen, C.; Elmegaard, B. Analysis of temperature glide matching of heat pumps with zeotropic working fluid mixtures for different temperature glides. *Energy* **2018**, *153*, 650–660. [CrossRef]
49. Su, W.; Hwang, Y.; Deng, S.; Zhao, L.; Zhao, D. Thermodynamic performance comparison of organic Rankine cycle between zeotropic mixtures and pure fluids under open heat source. *Energy Convers. Manag.* **2018**, *165*, 720–737. [CrossRef]
50. Andersen, W.C.; Bruno, T.J. Rapid screening of fluids for chemical stability in organic Rankine cycle applications. *Ind. Eng. Chem. Res.* **2005**, *44*, 5560–5566. [CrossRef]
51. Fabuss, M.A.; Borsanyi, A.S.; Fabuss, B.M.; Smith, J.O. Thermal stability studies of pure hydrocarbons in a high pressure isoteniscope. *J. Chem. Eng. Data* **1963**, *8*, 64–69. [CrossRef]
52. Keulen, L.; Gallarini, S.; Landolina, C.; Spinelli, A.; Iora, P.; Invernizzi, C.; Lietti, L.; Guardone, A. Thermal stability of hexamethyldisiloxane and octamethyltrisiloxane. *Energy* **2018**, *165*, 868–876. [CrossRef]
53. Di Marcoberardino, G.; Invernizzi, C.M.; Iora, P.; Arosio, L.; Canavese, M.; Lunghi, A.; Mazzei, A. Thermal stability and thermodynamic performances of pure siloxanes and their mixtures in organic Rankine cycles. *Energies* **2022**, *15*, 3498. [CrossRef]
54. Yu, W.; Liu, C.; Tan, L.; Li, Q.; Xin, L.; Wang, S. Thermal stability and thermal decomposition mechanism of octamethyltrisiloxane (MDM): Combined experiment, ReaxFF-MD and DFT study. *Energy* **2023**, *284*, 129289. [CrossRef]
55. Blake, E.S.; Hammann, W.C.; Edwards, J.W.; Reichard, T.E.; Ort, M.R. Thermal stability as a function of chemical structure. *J. Chem. Eng. Data* **1961**, *6*, 87–98. [CrossRef]
56. Johns, I.B.; McElhill, E.A.; Smith, J.O. Thermal stability of organic compounds. *Ind. Eng. Chem. Prod. Res. Dev.* **1962**, *1*, 2–6. [CrossRef]
57. Dai, X.; Shi, L.; An, Q.; Qian, W. Screening of hydrocarbons as supercritical ORCs working fluids by thermal stability. *Energy Convers. Manag.* **2016**, *126*, 632–637. [CrossRef]
58. Dai, X.; Shi, L.; Qian, W. Review of the working fluid thermal stability for organic Rankine cycles. *J. Therm. Sci.* **2019**, *28*, 597–607. [CrossRef]
59. Razafinarivo, N.; Bounaceur, R.; Burklé-Vitzthum, V.; Lannuzel, F.; Michels, R.; Scacchi, G.; Marquaire, P.M. Pyrolysis of n-octane at very low concentration and low temperature. *J. Anal. Appl. Pyrolysis* **2016**, *117*, 282–289. [CrossRef]
60. Macchi, E.; Astolfi, M. Axial flow turbines for Organic Rankine Cycle applications. In *Organic Rankine Cycle (ORC) Power Systems: Technologies and Applications*; Macchi, E., Astolfi, M., Eds.; Woodhead Publishing: Duxford, UK, 2017; pp. 299–319. [CrossRef]
61. *JCGM 100:2008*; Evaluation of Measurement Data—Guide to the Expression of Uncertainty in Measurement. Joint Committee for Guides in Metrology: Sèvres, France, 2008.
62. Hu, S.; Li, J.; Yang, F.; Yang, Z.; Duan, Y. Multi-objective optimization of organic Rankine cycle using hydrofluorolefins (HFOs) based on different target preferences. *Energy* **2020**, *203*, 117848. [CrossRef]
63. Myers, H.S. Binary mixtures of naphthenes and aromatics. *Ind. Eng. Chem.* **1956**, *48*, 1104–1108. [CrossRef]
64. Li, I.P.C.; Wong, Y.-W.; Chang, S.-D.; Lu, B.C.-Y. Vapor–liquid equilibria in systems n-hexane–benzene and n-pentane–toluene. *J. Chem. Eng. Data* **1972**, *17*, 492–498. [CrossRef]
65. Wu, X.; Chen, J.; Xie, L. Integrated operation design and control of Organic Rankine Cycle systems with disturbances. *Energy* **2018**, *163*, 115–129. [CrossRef]
66. Hu, D.; Zheng, Y.; Wu, Y.; Li, S.; Dai, Y. Off-design performance comparison of an organic Rankine cycle under different control strategies. *Appl. Energy* **2015**, *156*, 268–279. [CrossRef]

Disclaimer/Publisher's Note: The statements, opinions and data contained in all publications are solely those of the individual author(s) and contributor(s) and not of MDPI and/or the editor(s). MDPI and/or the editor(s) disclaim responsibility for any injury to people or property resulting from any ideas, methods, instructions or products referred to in the content.